

1 **The INFLUX Network – Eddy Covariance in and around an Urban Environment**

2

3 **Jason P Horne¹, Scott J Richardson¹, Samantha L Murphy¹, Helen C Kenion¹, Bernd J Haupt²,**
4 **Benjamin J Ahlswede¹, Natasha L Miles¹, Kenneth J Davis^{1,2}**

5 ¹Department of Meteorology and Atmospheric Science, The Pennsylvania State University,

6 University Park, 16802, PA, USA

7 ²Earth and Environmental Systems Institute, The Pennsylvania State University,

8 University Park, 16802, PA, USA

9 *Correspondence to:* Kenneth J Davis (kjd10@psu.edu)

10

11 **Abstract.** The eddy covariance method is used by various disciplines to measure atmospheric fluxes of
12 both vector and scalar quantities. One long-term, multi-site urban flux network experiment was the
13 Indianapolis Flux Experiment (INFLUX), which successfully deployed and operated eddy covariance
14 towers at eleven locations for varying deployment periods, measuring fluxes from land cover types within
15 and surrounding the urban environment in Indianapolis, Indiana, USA. The data collected from this
16 network of towers have been used to quantify urban greenhouse gas, energy, and momentum fluxes,
17 assess the performance of numerical weather and carbon cycle models, and develop new analysis
18 methods. This paper describes the available data associated with the INFLUX eddy covariance network,
19 provides details of data processing and quality control, and outlines the site attributes to assist in data
20 interpretation. For access to the various data products from the INFLUX eddy covariance work, please
21 see the data availability section below.

22

23 **Short summary.** We present data from a network of towers used to study the exchange of heat, water
24 vapor, and carbon dioxide between the surface and atmosphere in and around the city of Indianapolis, IN,
25 USA. We explain what was measured, how we checked data quality, and why these observations improve
26 our overall understanding of the urban environment.

27 1 Introduction

28

29 Eddy covariance (EC) is a method for quantifying atmospheric fluxes of mass, energy, and momentum.
30 EC measurements are commonly used to infer the exchange of these quantities between the Earth's
31 surface and the atmosphere. Using EC, investigators can monitor a system with minimal disturbance over
32 long periods, making it an attractive method for various disciplines (e.g., ecologists, meteorologists,
33 hydrologists) (Baldocchi et al., 2001). The technique is based on sampling the spectrum of turbulent
34 eddies and their associated scalar constituents to calculate the covariance between the vertical wind
35 component and the variable of interest. This covariance can be used to quantify the turbulent surface flux
36 of a variable (vector or scalar) in many conditions (e.g. Yi et al. 2000). The EC method typically uses
37 fast-response ($\geq 10\text{Hz}$) instruments to measure three-dimensional wind and various atmospheric scalars
38 (e.g., CO_2 , H_2O , temperature). A comprehensive description of the EC method can be found in Aubinet et
39 al. (2012) and Burba (2013) or many micrometeorological-focused texts (Foken, 2008; Lee et al., 2004).

40

41 Recent studies have employed an increasing number of EC measurements to study surface-atmosphere
42 fluxes across cities (Lipson et al., 2022; Nicolini et al., 2022; Papale et al., 2020). Nicolini et al. (2022)
43 compared thirteen EC towers in eleven different European cities to assess the impacts of the COVID-19
44 lockdown on CO_2 emissions. They found a significant relationship between factors such as the lockdown
45 stringency index (e.g., the Oxford Stringency Index) and the relative change in CO_2 flux (i.e., before vs.
46 during lockdown), demonstrating the value of EC measurements for detecting both long- and short-term
47 changes in CO_2 fluxes in real time. Jongen et al. (2022) used evapotranspiration measurements from EC
48 towers across twelve cities to infer water storage capacity. Their results show both variability in inferred
49 storage across the analyzed sites and a substantial difference between the estimated storage in urban areas
50 and storage reported in rural environments. The Urban-PLUMBER project ([https://urban-](https://urban-plumber.github.io/)
51 [plumber.github.io/](https://urban-plumber.github.io/)) gathered measurements from twenty flux towers located all over the world, creating a
52 dataset of urban EC measurements covering a spectrum of different climatic conditions and urban forms,
53 and has used these data for urban land surface model evaluation (Lipson et al., 2022). Other large-scale
54 efforts, such as the ICOS-Cities project, are expanding the number of EC measurements in the urban
55 environment. The FLUXNET project continues to bring together EC data into a globally-accessible
56 database.

57

58 Interpreting EC measurements in the urban environment is inherently difficult due to the high level of
59 heterogeneity (e.g., thermal and aerodynamic). This difficulty is not limited to EC but also applies to
60 many traditional micrometeorological theories and methods developed primarily for horizontally
61 homogeneous settings where horizontal spatial derivatives in the governing equation can be assumed
62 negligible. One approach to address this heterogeneity is to require deployments in seemingly
63 homogeneous urban areas where, for example, the EC flux footprint (i.e., the upwind area measured by
64 the EC system) envelops an area of roughly uniform surface characteristics and scalar source distributions
65 (Turnbull et al., 2025). When possible, this greatly simplifies data interpretation. This approach also
66 severely limits the number of viable EC measurement locations, most of which are seldom representative
67 of an urban mosaic, which, as stated, is often heterogeneous.

68

69 A contrasting and complementary approach is to deploy EC flux measurements in heterogeneous settings
70 and to adapt our analysis methods and theories to the inherently heterogeneous nature of the urban

71 environment. At least two issues emerge in this scenario. First, the EC flux measurements cannot be
72 interpreted in terms of a single set of land surface characteristics. EC measurements collected in
73 heterogeneous environments should be construed (at the very least) as a function of wind direction and
74 atmospheric stability conditions, ideally with a flux footprint model (e.g., Horst and Weil, 1992; Kljun et
75 al., 2015), and combined with data sets that can describe the urban landscape at a resolution that is finer
76 than the flux footprint. Such data analysis is complicated by the fact that typical flux footprint models
77 (e.g., Horst and Weil, 1992; Kljun et al., 2015) were developed for horizontally homogeneous
78 environments and should therefore be used with caution in highly heterogeneous systems.

79
80 Second, heterogeneity is ubiquitously associated with surface discontinuities, which are well understood
81 to give rise to rapidly evolving, non-equilibrium flow features such as internal boundary layers and
82 secondary circulations. Furthermore, in most real-world urban scenarios, these flow features merge and
83 interact, further complicating the problem (Bou-Zeid et al., 2020). For example, a secondary circulation
84 driven by spatial roughness or thermal differentials can result in non-negligible horizontal flux divergence
85 or mean advection (Feigenwinter et al., 2012), violating the one-dimensional, vertical transport, which is
86 typically used to infer surface-atmosphere exchange from EC flux measurements (Aubinet et al., 2012;
87 Burba, 2013). Diagnosing the presence of such flows can be attempted, for example, with multi-level
88 turbulent flux measurements (Yi et al., 2000). Yi et al. (2000) found only modest deviations from vertical-
89 only transport in a highly heterogeneous forested region. In other locations, however, heterogeneity-
90 induced secondary circulations have also been shown to impact EC measurements in arguably less
91 complex settings (compared to an urban setting) like agricultural fields (Eder et al., 2015a) and deserts
92 (Eder et al., 2015b), and have been linked to the lack of closure of the surface energy balance endemic to
93 EC flux measurements (Mauder et al., 2020). In summary, surface-atmosphere fluxes inferred from EC
94 flux measurements collected in heterogeneous urban environments should also be used with attention to
95 the inherent challenges and limitations.

96
97 Mixed sources further complicate the interpretation of urban EC flux measurements, as biological and
98 anthropogenic factors are often intertwined. The combined impacts of anthropogenic and biogenic
99 sources and sinks of CO₂ (Miller et al., 2020; Turnbull et al., 2019), sensible and latent heat (Ward et al.,
100 2022), and momentum (Kent et al., 2018) are measured by urban EC instruments. This complexity builds
101 on underlying mixtures of fluxes within natural (e.g., respiration [both heterotrophic and autotrophic] and
102 photosynthesis) and anthropogenic (e.g., vehicles and buildings; residential and industrial) systems.
103 Heterotrophic respiration of CO₂ by people should be approximately 0.24 μmol m⁻² s⁻¹ using population
104 densities for Indianapolis reported in the 2020 United States census (948 people km⁻²) and an average
105 respiration rate of 942 gCO₂ person⁻¹ day⁻¹ (Prairie and Duarte, 2007).

106
107 None of these challenges, however, are new or unique to urban systems, and all can be addressed through
108 ongoing research. Airborne EC has been conducted over heterogeneous flux footprints for decades
109 (Desjardins et al., 1992; Oncley et al., 1997), and flux footprint decomposition methods have been
110 employed for nearly as long (Schuepp et al., 1990; Mahrt et al., 2001). Footprint decomposition has been
111 used with tower-based EC to study natural (Wang et al., 2006; Xu et al., 2017) and anthropogenic (Dennis
112 et al., 2022; Wu et al., 2022) fluxes. Biological and anthropogenic CO₂ fluxes have been disaggregated in
113 the urban environment using both statistical partitioning methods (Crawford and Christen 2015; Lee et al.
114 2021; Menzer and McFadden 2017) and tracer ratio methods (Ishidoya et al. 2020; Wu et al. 2022).

115 Complex ecosystem flux sites (e.g., Davis et al., 2003) have served as a guide for flux upscaling studies
116 (Wang et al., 2006; Xiao et al., 2014), and all sites in the Americas flux tower network (Ameriflux,
117 Novick et al., 2018) have been categorized according to their degree of heterogeneity (Chu et al., 2021).
118 Lateral flow in low turbulence conditions has been recognized as a problem in all EC deployments (Barr
119 et al., 2013). Landscape-scale secondary circulations have been investigated in agricultural (Kang et al.,
120 2007) and forested landscapes (Butterworth et al., 2021). Given that urban environments are where over
121 55% (and rising) of the global population lives (Sun et al., 2020) and given the past successes in studying
122 complex micrometeorological environments, we would like to stress the importance of understanding
123 these complex systems and moving ahead with measurements that go beyond the classic homogeneous
124 flux tower site.

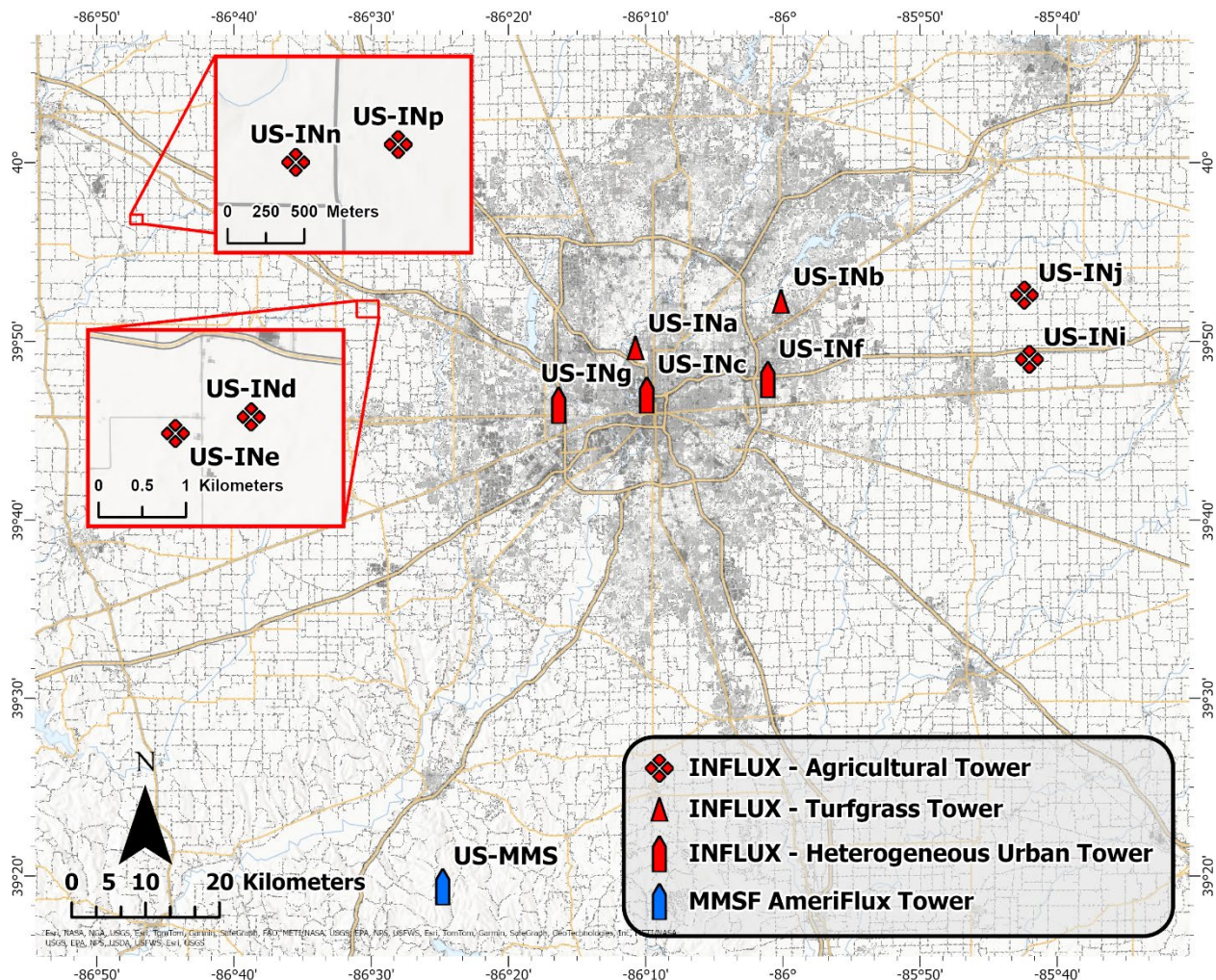
125
126 Many efforts have successfully measured fluxes using EC in the urban environment (Biraud et al., 2021;
127 Kotthaus and Grimmond, 2014; Menzer and McFadden, 2017; Vogt et al., 2006; Wu et al., 2022). Urban
128 greenhouse gas (GHG) emissions are a common focus of these efforts. Urban areas are responsible for
129 67-72% of anthropogenic CO₂ emissions globally (Lwasa et al., 2023). Many cities have pledged to
130 reduce GHG emissions amid anthropogenic climate change, for example, initiatives like NetZeroCities
131 (European Union, 2025) or the Covenant of Mayors (Kona et al., 2018). The EC method can directly
132 measure GHG fluxes within the tower's footprint and reveal the urban metabolism. Liu et al. (2012)
133 investigated spatial and temporal variability of CO₂ fluxes in the Beijing megacity using the EC method
134 and found weekly (e.g., traffic volume) and seasonal (e.g., domestic heating) patterns in CO₂ fluxes.
135 Crawford and Christen (2015) were able to disaggregate observed CO₂ fluxes into biogenic and
136 anthropogenic sources by modeling various sources/sinks within the turbulent source area (i.e., flux
137 footprint) of a residential area in Vancouver, Canada. Similar work by Stagakis et al. (2019) disaggregated
138 measured CO₂ fluxes in the Mediterranean city of Heraklion, Greece, using source-area modeling and
139 high-resolution geospatial descriptions of the surrounding urban areas, finding high overall annual
140 emissions compared with other EC-derived estimates from other cities. Pawlak and Fortuniak (2016)
141 assessed the temporal variability of CH₄ fluxes in a populated area of Łódź, Poland, and found the city's
142 annual emissions were comparable to surrounding natural sources like wetlands. Menzer and McFadden
143 (2017) used statistical partitioning of CO₂ fluxes over a suburban neighborhood outside Saint Paul,
144 Minnesota (US-KUO: KUOM tower) to separate biogenic from anthropogenic sources.

145
146 Recently, intra-urban networks have begun to emerge. Multiple towers within and outside a single city
147 enable a more detailed understanding of the urban system than could be achieved with a single flux tower.
148 For example, Nicolini et al. (2022) were able to use paired towers within the same city (e.g., residential
149 vs. non-residential) to infer qualitative information on the dominant CO₂ driver (e.g., vehicular,
150 vegetation, etc.). Peters et al. (2011) showed the benefit of measuring turfgrass lawns using a short-stature
151 (1.35 m) tower to help interpret evapotranspiration (ET) measurements made on the collocated KUOM
152 tower (40 m) in Saint Paul, Minnesota. In recent years there has been an expansion of urban EC in the
153 United States through projects like the Indianapolis Flux Experiment (INFLUX, Davis et al., 2017), the
154 Baltimore Social and Environmental Collaborative (BSEC), the Coastal Rural Atmospheric Gradient
155 Experiment (CoURAGE, Davis et al., 2024), the Community Research on Climate and Urban Science
156 (CROCUS, Raut et al., 2025), and the Southwest Urban Integrated Field Laboratory (SW-IFL, 2024).

157

158 INFLUX was a contribution to the urban greenhouse gas test beds program of the National Institute of
159 Standards and Technology (Semerjian and Whetstone, 2021). This program endeavored to “improve
160 emission measurement tools to better equip decision makers and mitigation managers with capabilities to
161 chart progress in GHG emissions mitigation” ([https://www.nist.gov/greenhouse-gas-measurements/urban-
162 test-beds](https://www.nist.gov/greenhouse-gas-measurements/urban-test-beds)). The INFLUX project was the longest-running test bed in this program. Atmospheric inversions
163 were the primary technological approach employed for urban GHG emissions estimates in the test bed
164 program (Karion et al., 2023; Lauvaux et al., 2020; Yadav et al., 2023), given their ability to encompass
165 emissions from the entirety of an urban area. Atmospheric inversions struggle, however, to infer the
166 spatial structure of emissions within a city (e.g. Lauvaux et al., 2020). EC flux towers, long used to study
167 fluxes at a spatial resolution more accessible to local-scale, process-based model evaluation, have been
168 deployed in INFLUX to complement whole-city atmospheric inversions.

169
170 The INFLUX EC flux towers measured CO₂, H₂O, energy, and momentum fluxes in and around
171 Indianapolis. The network included EC flux observations from eleven locations (Fig. 1), comprising over
172 a decade and a half of observation site years (Table 1, Fig. 2). These tower locations range from
173 agricultural sites in the croplands surrounding Indianapolis to towers in the cities’ interior over turfgrass,
174 suburban forests, residential areas, and heavily developed urban regions (Fig. 1). This multiplicity of flux
175 sites was achieved by moving instrumentation from site to site as deemed necessary to sample the
176 variability in fluxes in and around this urban landscape. A subset of the flux measurements (Table 1) have
177 been co-located with mole fraction observations (Richardson et al., 2017) from the INFLUX urban GHG
178 testbed monitoring network (Miles et al., 2017a).



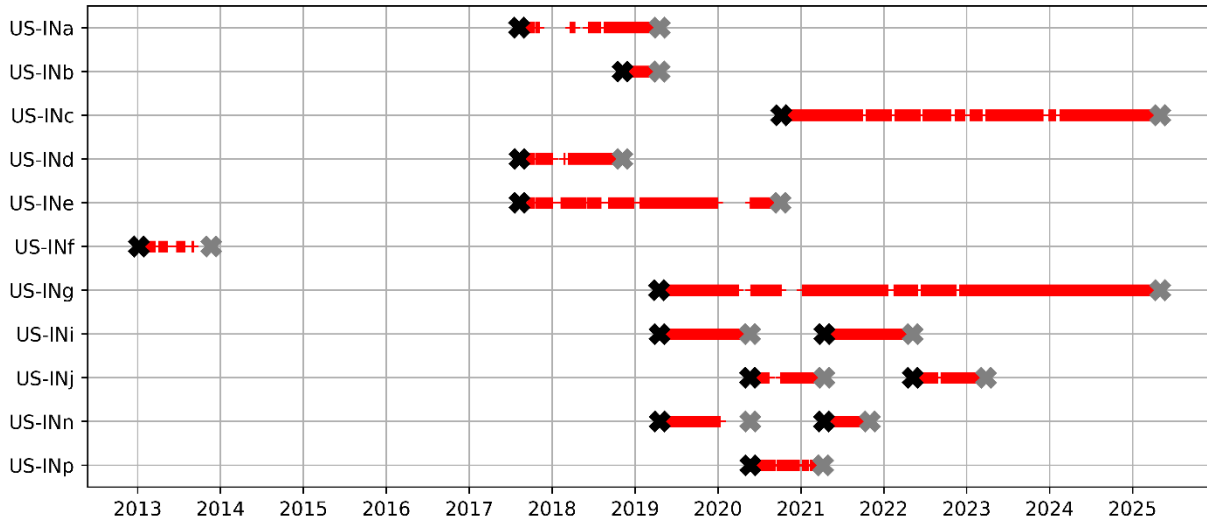
179
 180 **Figure 1.** Locations of INFLUX eddy covariance towers in and around Indianapolis, IN. Specific flux
 181 tower site locations (i.e., latitude and longitude) are included in the site metadata file with the processed
 182 data files. The gray shading represents the 2023 impervious surface cover from the National Land Cover
 183 Database (doi.org/10.5066/P9JZ7AO3). Major roadways are depicted using orange lines, and waterways
 184 are shown in light blue. The Morgan-Monroe State Forest (MMSF) AmeriFlux tower is also included for
 185 spatial reference. Service layer credits go to City of Indianapolis, Marion County, Esri, TomTom,
 186 Garmin, SafeGraph, FAO, METI/NASA, USGS, EPA, NPS, USFWS, and GeoTechnologies Inc.

187
 188 **Table 1.** Site identification in FLUXNET format, deployment period, and a short description of each site.

Site – Category	Time Start	Time End	Site Description
US-INa – Turfgrass	August 2017	April 2019	Pioneer Cemetery in Crown Hill Cemetery tower measured a minimally managed turfgrass lawn—primarily cool-season C3 grass species.
US-INb – Turfgrass	November 2018	April 2019	The Fort Golf Resort tower was located on a heavily managed turfgrass lawn—primarily cool-season C3 grass species.

US-INc – Heterogeneous Urban	October 2020	May 2025	The downtown Indianapolis tower measured an urbanized, heterogeneous area and is also a mole fraction site 03*.
US-INd – Agricultural	August 2017	November 2018	Agricultural tower near Pittsboro measured a mixture of corn and soy.
US-INe – Agricultural	September 2017	October 2020	Agricultural tower near Pittsboro measured corn (2018 and 2020) and soy (2019).
US-INf – Heterogeneous Urban	January 2013	November 2013	The tower at East 21st St lies within a heterogeneous commercial and residential area and corresponds to the mole fraction site 02*.
US-ING – Heterogeneous Urban	April 2019	May 2025	Wayne Twp Comm tower is located in a heterogeneous residential and commercial area and is also a mole fraction site 07*.
US-INi – Agricultural	April 2019	May 2022	Agricultural tower measured soy (2019) and corn (2021). Located near the mole fraction site 09*.
US-INj – Agricultural	May 2020	March 2023	Agricultural tower measured corn during both growing seasons (2020 and 2022). Located near mole fraction site 09*.
US-INn – Agricultural	April 2019	October 2021	Agricultural tower measured corn during 2019 and 2021. Located near mole fraction site 14*.
US-INp – Agricultural	May 2020	April 2021	Agricultural tower measured a mixture of corn and turfgrass in 2020. Located near mole fraction site 14*.

189 * Mole fraction towers and their numbers are described in Miles et al. (2017a).



190
 191 **Figure 2:** Data availability at each site through the timeline of the INFLUX project. Each half-hour data
 192 point is indicated by a red “+”, flux instrumentation deployment dates are indicated by black x’s, and flux
 193 instrumentation decommissioning dates are indicated by gray x’s. Any missing data between the
 194 deployment and decommissioning dates is due to power loss or instrument malfunction.

195 This paper documents the urban EC measurements undertaken as part of the INFLUX project. We discuss
 196 methods for quality-controlling the INFLUX EC measurements and describe the groups of EC flux sites
 197 within the INFLUX project (i.e., agricultural, turfgrass, and heterogeneous urban towers). We present the
 198 data processing required to interpret the data within this urban network and document the availability of
 199 data products.

200 **2 INFLUX Eddy Covariance Tower Network**

201 **2.1 General Climate**

202
 203 The INFLUX project is based in and around Indianapolis, IN, USA. The city of Indianapolis and the
 204 surrounding area are on the boundary of two Köppen climate classifications, Dfa and Cfa (Kottek et al.,
 205 2006) at an elevation of approximately 220 m above sea level. We reference data from the National
 206 Oceanic and Atmospheric Administration's (NOAA) National Centers for Environmental Information
 207 (NCEI) to provide averages for the period between 1991 and 2025. Indianapolis receives, on average,
 208 approximately 111 cm of liquid precipitation and 65 cm of snowfall (depth) annually. The annual average
 209 daily high and low temperatures are 17°C and 7°C, respectively.

211 **2.2 Flux tower sites and site categories**

212
 213 The INFLUX flux towers can be subdivided into heterogeneous (US-INc, US-ING, US-INF) and
 214 homogeneous sites. Within the homogeneous grouping, we further subdivide the towers into agricultural
 215 (US-INd, US-INE, US-INi, US-INj, US-INn, US-INp) and turfgrass (US-INa, US-INb) categories. Each
 216 site is equipped with a sonic anemometer, either a Gill WindMaster (WindMaster, Gill Instruments,
 217 Lymington, UK) or CSAT3 (CSAT3, Campbell Scientific, Logan, UT, USA), and an infrared gas

218 analyzer (LI-7500DS or LI-7500A, LI-COR Biosciences, Lincoln, NE, USA) collecting data at 10Hz
 219 frequency (Table 2). The low-stature towers are also equipped with a temperature and humidity probe
 220 (HMP155, Vaisala Oyj, Vantaa, Finland), and a subset of them are equipped with photosynthetically
 221 active radiation (PAR) sensors (LI190R, LI-COR Biosciences, Lincoln, NE, USA) (Table 2). US-INc and
 222 US-INg were equipped with 4-way net radiometers (CNR4, Kipp and Zonen, Delftechpark, Netherlands)
 223 in October 2023 and March 2024, respectively. In addition to the INFLUX EC towers, the AmeriFlux
 224 Core Site US-MMS (Fig. 1), located in the Monroe-Morgan State Forest, is approximately seventy
 225 kilometers to the southwest of Indianapolis (Dragoni et al., 2011; Schmid et al., 2000).

226
 227 **Table 2.** Measurement heights of deployed eddy covariance instruments and flux instruments for each
 228 site.

Site – Category	EC measurement height AGL	Infrared gas analyzer	Sonic anemometer	Temperature/ Humidity	PAR	Net Radiation	Arable
US-INa – Turfgrass	3 m	Licor LI-7500A	Campbell CSAT3	Vaisala HMP155	-	-	-
US-INb – Turfgrass	3 m	Licor LI-7500A	Campbell CSAT3	Vaisala HMP155	-	-	-
US-INc – Mixed Urban	43 m	Licor LI-7500A	Campbell CSAT3	-	-	Kipp & Zonen CNR4 (10/2023)	-
US-INd – Agricultural	3 m	Licor LI-7500A	Campbell CSAT3	Vaisala HMP155	-	-	-
US-INe – Agricultural	3 m	Licor LI-7500A	Campbell CSAT3	Vaisala HMP155	-	-	Yes
US-INf – Mixed Urban	30 m	Licor LI-7500A	Campbell CSAT3	-	-	-	-
US-INg – Mixed Urban	41 m	Licor LI-7500DS	Gill WindMaster	-	-	Kipp & Zonen CNR4 (03/2024)	-
US-INi – Agricultural	3 m	Licor LI-7500A	Campbell CSAT3	Vaisala HMP155	Licor LI190R	-	-
US-INj – Agricultural	3 m	Licor LI-7500A	Campbell CSAT3	Vaisala HMP155	Licor LI190R	-	Yes
US-INn – Agricultural	3 m	Licor LI-7500A	Campbell CSAT3	Vaisala HMP155	Licor LI190R	-	-
US-INp – Agricultural	3 m	Licor LI-7500A	Campbell CSAT3	Vaisala HMP155	-	-	Yes

229
 230 **2.3 Data acquisition and organization**
 231

232 The INFLUX EC instruments produce continuous time-series measurements, which are separated into
233 individual GHG data files (.ghg) containing 30 minutes of continuous data, for a total of 48 files per day.
234 Each GHG file is transferred from the logger to a Linux server using the Secure Socket Shell (SSH) file
235 transfer protocol. Each instrument has a unique incoming directory where the files are stored. Every night,
236 a set of shell scripts checks to see if all 48 files have been delivered. Furthermore, every night, GHG files
237 are copied to an archive while the data files are checked for (i) readability for further processing
238 (occasionally some files are corrupt), (ii) monotonic time increase of recorded data (will be automatically
239 corrected if possible), (iii) any non-ASCII characters which could cause problems during further scientific
240 processing), (iv) incomplete data rows. Emails are automatically generated if any fault is recognized,
241 while copies of the automatically modified and corrected data files are saved. Each step is captured in a
242 log file. Missing data, errors, and file modifications due to errors trigger an email notification. These
243 checks test file integrity and data completeness. Once the integrity tests are completed, the data is
244 automatically processed and analyzed using EddyPro (LI-COR, 2021) and a set of Python scripts.
245 Graphics of the processed data (a two-week data window) are automatically updated online, allowing for
246 manual monitoring of the incoming data and quick identification and resolution of issues. This allows
247 researchers to quickly determine whether the instruments produce reasonable results or require immediate
248 attention.

249

250 **2.4 Flux processing and quality control**

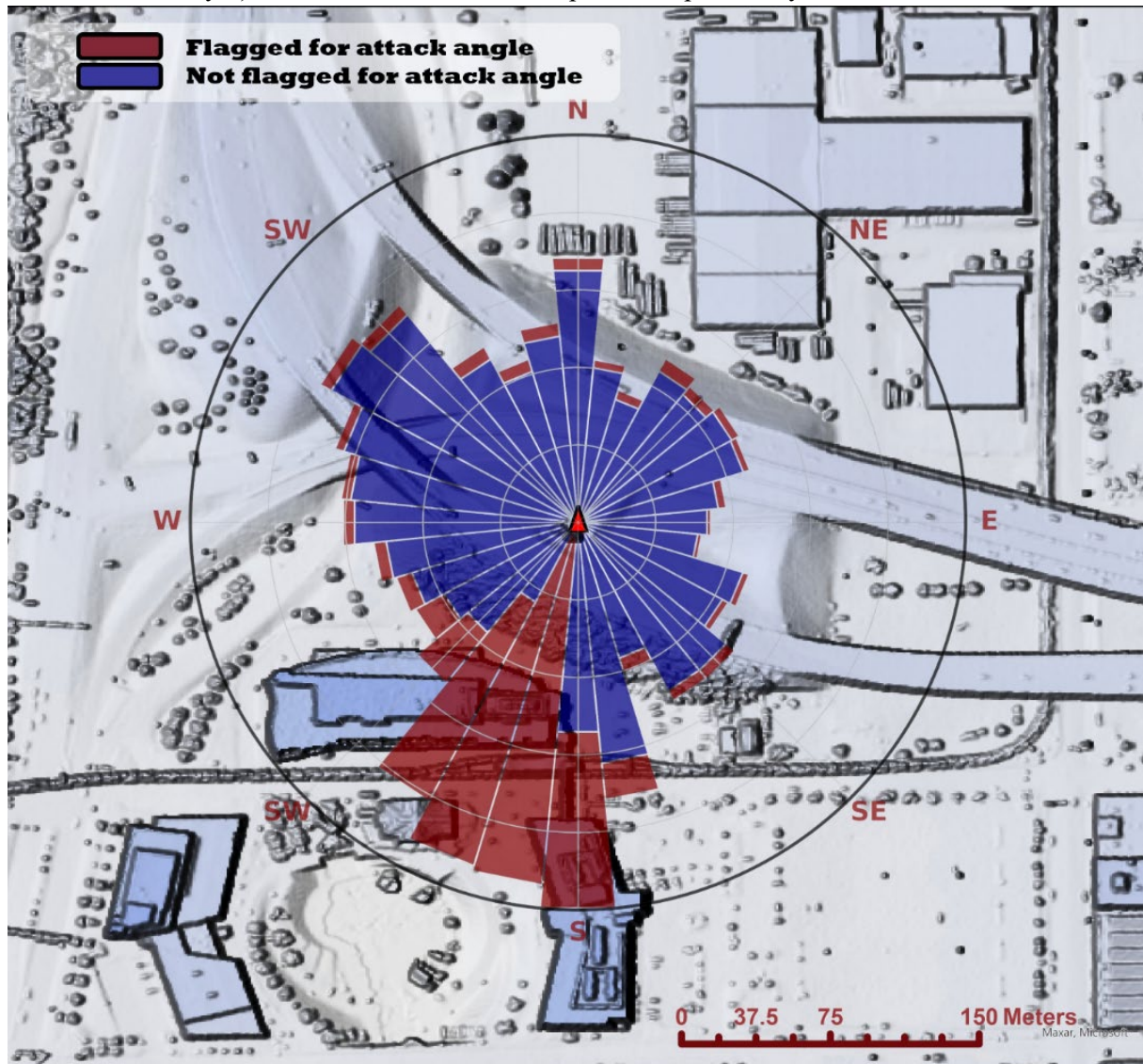
251

252 The complete time series of fluxes is calculated separately from the automatic processing script using a
253 set of distinct post-processing steps and the EddyPro software package. For a comparison between
254 EddyPro and other commonly used software (e.g., TK3 and eddy4R) when processing fluxes at
255 heterogeneous urban flux towers, please see Lan et al. (2024). For every thirty minutes, we apply a block-
256 averaging detrending (Foken, 2008; Lee et al., 2004) and planar fit coordinate rotation (Lee et al., 2004;
257 Paw U et al., 2000; Wilczak et al., 2001). The Vickers and Mahrt (1997) despiking procedure is
258 performed before calculating fluxes, spikes are removed, and the number of spikes is reported. As the
259 molar densities are measured by open-path sensors (LI-7500A or LI-7500DS), we apply the Webb,
260 Pearman, and Leuning correction for density fluctuations (Lee and Massman, 2011; Paw U et al., 2000;
261 Webb et al., 1980) following the iterative methodology employed in EddyPro. The cospectra are corrected
262 (high and lowpass) via the analytical methods of Moncrieff et al. (1997), which is based on the methods
263 of Moore (1986) using the similarity-based cospectral models from Kaimal et al. (1972). For each
264 averaging period, using the methods of Vickers and Mahrt (1997), a set of flags is generated based on the
265 high-frequency measurements. The deployment at Site US-INF was a preliminary effort that did not
266 follow these same procedures. We employed a locally written EC code (Shi et al., 2013) that includes
267 planar fit rotation and Vickers and Mahrt (1997) despiking algorithms. Due to differences in the data
268 acquired for this system, we were unable to apply the data processing used for the remaining INFLUX
269 towers. The US-INF data are described in more detail in Sarmiento et al. (2017) and Wu et al. (2022).

270

271 Flux data are flagged for violating an angle of attack test if $>10\%$ of the wind vectors exceed an attack
272 angle of $>|30^\circ|$ for the averaging period. In the urban environment, the attack angle can be used to
273 examine the impact of wake turbulence generated by roughness elements (RE) within the tower's
274 footprint. For example, wind directions from the southwest ($180-225^\circ$) of Site US-INc (Fig. 3) are flagged
275 $\geq 30\%$ of the time, detecting wake turbulence generated by a 30 m tall building 100 m southwest of the

276 tower. From these impacted wind directions, the measured fluxes are not within the inertial sublayer (i.e.,
277 the constant flux layer), where traditional EC assumptions are potentially valid.



278
279 **Figure 3.** Percent of total data (i.e., all wind directions) flagged (radial) as a binary attack angle flagging
280 (red/blue) vs. wind direction (angular) at US-INc (Oct 2020 – Jan 2023). Radial scales show 1.1, 2.2, 3.3,
281 4.4, and 5.6 percent of the total data moving from the inner to the outer ring, respectively. The red triangle
282 represents the location of US-INc. The base map is a digital surface map generated using 2016 Indiana
283 Statewide 3DEP LiDAR Data Products for Marion County (USDA, 2016). Service layer credits go to
284 Maxar and Microsoft.

285
286 Fluxes are also flagged using a suite of quality control tests available through EddyPro, which are
287 commonly used in EC research. Stationarity tests are conducted for each half-hour using the methodology
288 of Foken and Wichura (1996) and Vickers and Mahrt (1997). Modeled integral turbulence characteristics
289 from flux variance similarity theory are compared to measured variances of winds and scalars using the
290 methods of Foken and Wichura (1996). Depending on the degree of nonstationarity and deviation from
291 flux similarity theory, as determined by the Foken and Wichura (1996) tests, each averaging period is

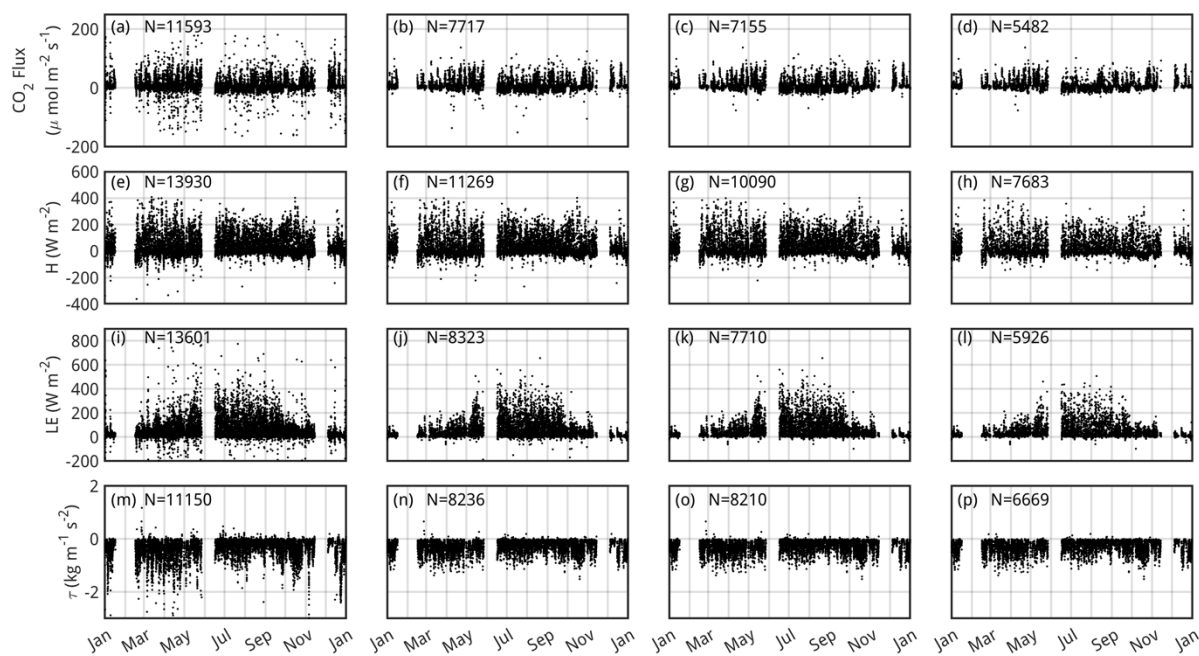
292 assigned a value (1-9) based on the scheme of Mauder and Foken (2004). When comparing measurements
293 made at the heterogeneous urban towers to similarity predictions, it is worth noting that aerodynamic
294 parameters, such as displacement height, are often directionally dependent (Kent et al., 2018). Thus, the
295 similarity-based relationship should scale differently depending on the wind direction. Subtle details, such
296 as these, are not included in the current version of EddyPro, but the software's default flags, generated (as
297 discussed here), can still guide users in interpreting the data.

298
299 For two agricultural sites, US-INn and US-INp, periods of the high-frequency data were lost, and only a
300 version of the processed thirty-minute data using the default EddyPro settings was recovered. At US-INn,
301 the period is from April 21, 2019, 00:00 UTC to January 10, 2020, 03:30 UTC, and at US-INp, it is from
302 May 23, 2020, 21:30 UTC to December 22, 2020, 16:00 UTC. For these periods when high-frequency
303 data were lost, fluxes are calculated using a double-coordinate rotation and flagged according to a
304 simplified version of the 1-9 scheme, as outlined in the Spoleto agreement of 2004 for CarboEurope-IP,
305 as described in Mauder and Foken (2004). These periods of missing high-frequency data have been
306 combined with those where the high-frequency data is available, resulting in a mixture of flagging
307 schemes and coordinate rotation in some columns.

308
309 After calculating half-hourly fluxes, additional screening methods generate flags for periods with weak
310 gas-analyzer signals, extreme flux values, or inadequate mechanical mixing during nocturnal periods. The
311 data are flagged if the signal strength reported by the gas analyzer over a half-hour period falls below the
312 mean signal strength for a two-week moving window. Nighttime data (i.e., periods when the solar altitude
313 is $\leq 0^\circ$) are flagged during low-turbulence periods using the methods of Goulden et al. (1996). We
314 acknowledge that the use of friction velocity filters in urban areas is still under question (Papale et al.,
315 2022); a consensus has not been reached. We assert that this remains a valuable screening tool for these
316 datasets. Finally, the flux data are flagged based on a threshold of N standard deviations from the mean,
317 where N is a site-specific number chosen to keep flux magnitudes within geophysical limits. While the
318 standard deviation and signal strength flag perform well at identifying potentially erroneous flux
319 calculations, it should be noted that these quality control procedures are imperfect (as with the quality
320 control methods mentioned) and could flag legitimate flux measurements.

321
322 We provide processed, half-hourly flux datasets for each of the eleven INFLUX sites through Penn State
323 Data Commons and Ameriflux (See Section 3). Included with these data are metadata files with
324 information on details such as flagging thresholds (e.g., friction velocity threshold) or site geographic
325 coordinates. We do not remove data based on the generated flags for the data set available on Penn State
326 Data Commons; instead, we leave the filtering decisions to the users. For most use cases, we do not
327 recommend eliminating all points flagged using the quality control flags provided by the methods of
328 Vickers and Mahrt (1997) and Mauder and Foken (2004), as a large proportion of physically reasonable
329 data is flagged. We give an example of four different quality control flag combinations for CO₂, latent
330 heat, sensible heat, and momentum fluxes using observations at Site US-INg in Fig. 4. The four quality
331 control flag combinations for each of these fluxes are summarized in Table 3. We recommended at
332 minimum filtering the data according to friction velocity and CO₂ flux standard deviation flags for
333 analysis of CO₂ fluxes, sensible heat standard deviations flags for analysis of sensible heat fluxes, latent
334 heat standard deviation flags for analysis of latent heat fluxes, and removing wind directions from which
335 the measurement is impact by distortion due to the tower (for Site US-INg, observations from wind

336 directions 30-135° should be removed) for momentum fluxes (Set 1 in Table 3). From wind directions
 337 where the towers distort the flow, we do not observe a clear impact on scalar fluxes; thus, we leave the
 338 decision for removal to the data user. To remove additional outlier points, we suggest filtering by Sets 2 or
 339 3 (Table 3) as shown in Fig. 4b and Fig. 4c for CO₂ fluxes, Fig. 4f and Fig. 4g for sensible heat fluxes,
 340 Fig. 4j and Fig. 4k for latent heat fluxes, and Fig. 4n and Fig. 4o for momentum fluxes. Given the
 341 significant reduction of overall data points, we do not suggest the flagging combination of Set 4, as shown
 342 in Fig. 4d, h, l, and p, unless the application of the data requires the strictest turbulence screening, which
 343 is appropriate only if the most idealized conditions for EC flux measurements are needed. At the
 344 heterogeneous urban flux towers (US-INc and US-INg), we recommend not removing scalar flux data
 345 based on the Vickers and Mahrt (1997) higher-moment statistics (i.e., skewness and kurtosis), as these
 346 flags commonly target realistic data at these sites (Järvi et al., 2018). This is due to the spatial and
 347 temporal heterogeneity of the urban environment, which can cause the distribution of high-frequency
 348 scalar measurements for a single period often to exceed the default skewness or kurtosis thresholds in
 349 EddyPro.



350 **Figure 4.** CO₂ fluxes (panels (a)-(d)), sensible heat fluxes (H) (panels (e)-(h)), latent heat fluxes (LE)
 351 (panels (i)-(l)), and momentum fluxes (τ) (panels (m)-(p)) at Site US-INg for 2022 with different quality
 352 control flags applied. From left to right, the filtering sets 1, 2, 3, and 4 (see Table 3 for full set
 353 descriptions) are shown for each of the fluxes, representing a range of filtering choices from least to most
 354 stringent. The number of points remaining in the dataset after removing quality control flags is indicated
 355 on each panel. With no filtering applied, there are 13,779 CO₂ flux data points, 13,969 sensible heat data
 356 points, 13,697 latent heat flux data points, and 13,969 momentum flux data points. For filtering Sets 1, 2,
 357 3, and 4, respectively, 84.1%, 56.0%, 51.9%, and 39.7% of the total CO₂ flux data are preserved, 99.7%,
 358 80.6%, 72.2%, and 55.0% of sensible heat flux data are preserved, 99.2%, 60.7%, 56.2%, and 43.2% of
 359 latent heat flux data are preserved, and 79.8%, 58.9%, 58.7% and 47.7% of momentum flux data are
 360 preserved, and 79.8%, 58.9%, 58.7% and 47.7% of momentum flux data are
 361 preserved.

362 **Table 3:** Description of quality control flag combinations considered for CO₂, sensible heat (H), latent
 363 heat (LE), and momentum (τ) fluxes. The hard flag is abbreviated as 'hf' in the table.

Flux	Set 1	Set 2	Set 3	Set 4
CO₂	Friction velocity	Friction velocity	Friction velocity	Friction velocity
	CO ₂ flux standard deviation			
		Spike hf w	Spike hf w	Spike hf w
		Amplitude resolution hf w	Amplitude resolution hf w	Amplitude resolution hf w
		Drop out hf w	Drop out hf w	Drop out hf w
		Absolute limits hf w	Absolute limits hf w	Absolute limits hf w
		Discontinuities hf w	Discontinuities hf w	Skewness and kurtosis hf w
		Spike hf CO ₂	Spike hf CO ₂	Discontinuities hf w
		Amplitude resolution hf CO ₂	Amplitude resolution hf CO ₂	Spike hf CO ₂
		Drop out hf CO ₂	Drop out hf CO ₂	Amplitude resolution hf CO ₂
		Absolute limits hf CO ₂	Absolute limits hf CO ₂	Drop out hf CO ₂
		Discontinuities hf CO ₂	Discontinuities hf CO ₂	Absolute limits hf CO ₂
		Signal strength	Signal strength	Discontinuities hf CO ₂
			CO ₂ QC greater than 5	Signal strength
			CO ₂ QC greater than 5	
			Attack angle hf	
			Nonsteady wind hf	
H	H standard deviation	H standard deviation	H standard deviation	H standard deviation
		Spike hf w	Spike hf w	Spike hf w
		Amplitude resolution hf w	Amplitude resolution hf w	Amplitude resolution hf w
		Drop out hf w	Drop out hf w	Drop out hf w
		Absolute limits hf w	Absolute limits hf w	Absolute limits hf w
		Discontinuities hf w	Discontinuities hf w	Skewness and kurtosis hf w
			H QC greater than 5	Discontinuities hf w
			H QC greater than 5	
			Attack angle hf	
			Nonsteady wind hf	
LE	H ₂ O flux standard deviation			
		Spike hf w	Spike hf w	Spike hf w
		Amplitude resolution hf w	Amplitude resolution hf w	Amplitude resolution hf w
		Drop out hf w	Drop out hf w	Drop out hf w
		Absolute limits hf w	Absolute limits hf w	Absolute limits hf w

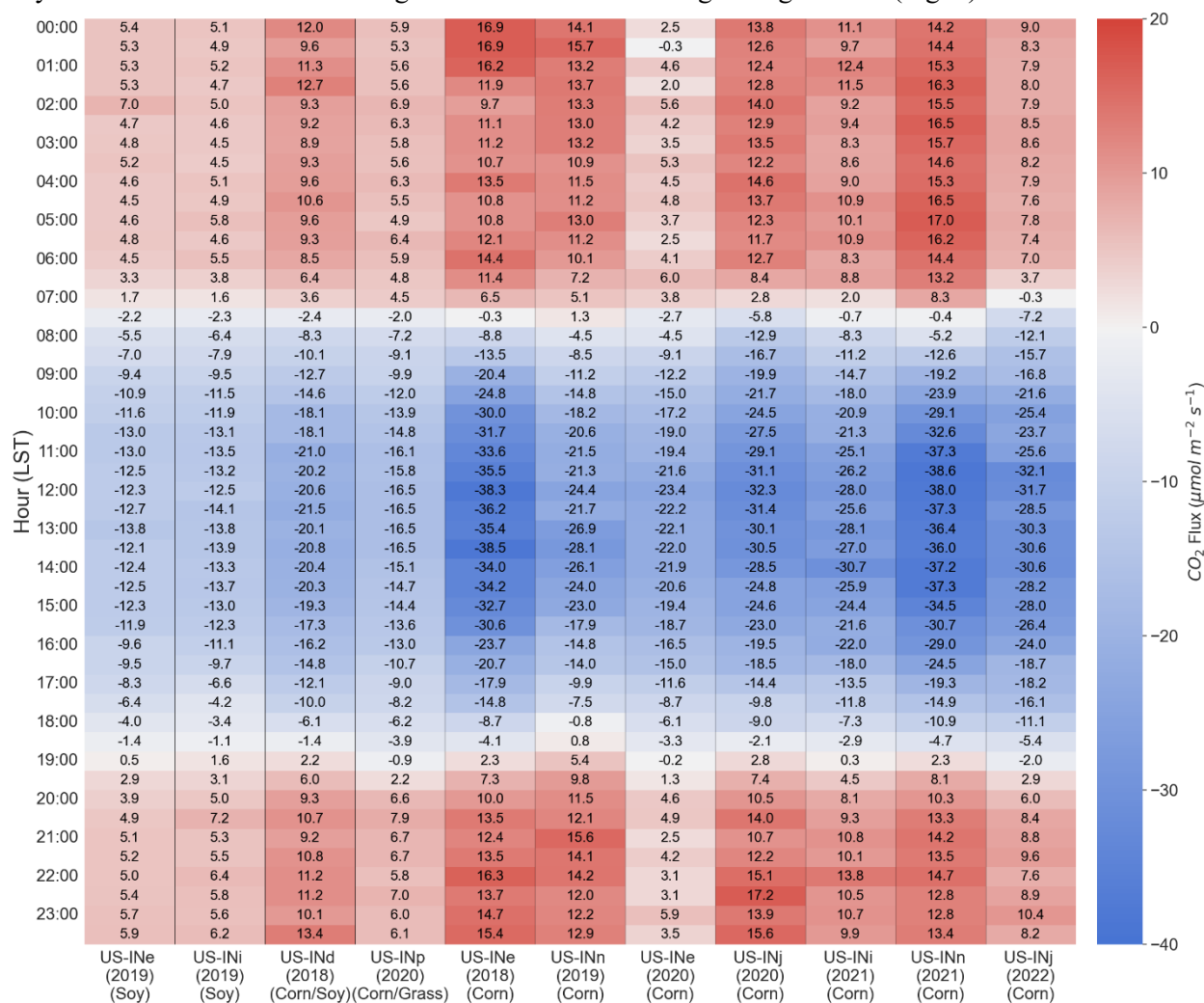
		Discontinuities hf w Spike hf H ₂ O Amplitude resolution hf H ₂ O Drop out hf H ₂ O Absolute limits hf H ₂ O Skewness and kurtosis hf H ₂ O Signal strength	Discontinuities hf w Spike hf H ₂ O Amplitude resolution hf H ₂ O Drop out hf H ₂ O Absolute limits hf H ₂ O Skewness and kurtosis hf H ₂ O Signal strength LE QC greater than 5	Skewness and kurtosis hf w Discontinuities hf w Spike hf H ₂ O Amplitude resolution hf H ₂ O Drop out hf H ₂ O Absolute limits hf H ₂ O Skewness and kurtosis hf H ₂ O Signal strength LE QC greater than 5 Attack angle hf Nonsteady wind hf
τ	Wind directions impacted by tower distortion	Wind directions impacted by tower distortion Spike hf w Amplitude resolution hf w Drop out hf w Absolute limits hf w Discontinuities hf w Spike hf v Amplitude resolution hf v Drop out hf v Absolute limits hf v Discontinuities hf v Spike hf u Amplitude resolution hf u Drop out hf u Absolute limits hf u Discontinuities hf u Attack angle hf	Wind directions impacted by tower distortion Spike hf w Amplitude resolution hf w Drop out hf w Absolute limits hf w Discontinuities hf w Spike hf v Amplitude resolution hf v Drop out hf v Absolute limits hf v Discontinuities hf v Spike hf u Amplitude resolution hf u Drop out hf u Absolute limits hf u Discontinuities hf u QC τ greater than 5 Attack angle hf	Wind directions impacted by tower distortion Spike hf w Amplitude resolution hf w Drop out hf w Absolute limits hf w Skewness and kurtosis hf w Discontinuities hf w Spike hf v Amplitude resolution hf v Drop out hf v Absolute limits hf v Skewness and kurtosis hf v Discontinuities hf v Spike hf u Amplitude resolution hf u Drop out hf u Absolute limits hf u Skewness and kurtosis hf u Discontinuities hf u QC τ greater than 5 Attack angle hf Nonsteady wind hf

364

365 2.5 Agricultural Sites

366

367 Understanding the boundary layer dynamics and CO₂ fluxes surrounding a city is important for
 368 understanding measurements collected within the city. The area surrounding Indianapolis is mainly
 369 composed of agricultural fields planted with a rotation of corn and soybeans. We deployed short-stature
 370 (~3 m AGL) flux towers at six locations in agricultural fields within 30-60 km of downtown Indianapolis
 371 (Fig. 1). The instrumentation for the agricultural sites was, in most cases, relocated annually to sample a
 372 variety of fields (specifically US-INd, US-INe, US-INn, US-INp). Each location was given a different site
 373 key. We collected data at the six agricultural sites for eleven growing seasons (Fig. 5).



374 **Figure 5.** The average summer (JJA) diel cycle of CO₂ fluxes for each agriculture site-year. Each column
 375 is also labeled with the surrounding vegetation. The numbers indicate the average half-hour flux for each
 376 underlying color.
 377

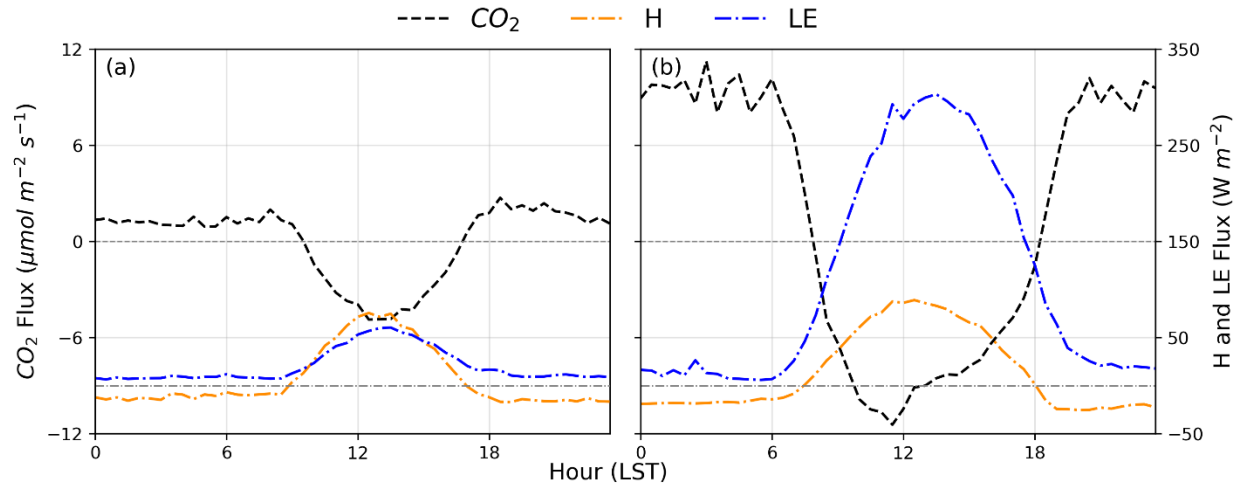
378 Flux footprint analyses are used to identify averaging periods when these agricultural towers may have
 379 been strongly influenced by vegetation other than the crops to be sampled. These conditions arise from
 380 the practical limitation of placing the flux towers close to, but not directly within, the actively managed

381 fields, meaning that at times the towers were located at the boundary between two adjacent crop types.
382 The fractional coverage of the agricultural crop of interest (corn or soybean) within the estimated tower
383 footprint was calculated for each agricultural flux site in the INFLUX network. The calculated fractional
384 coverage values allow a data user to select thresholds for which they would consider the half-hourly flux
385 value representative of the vegetation of interest. The Flux Footprint Prediction (FFP) model, developed
386 by Kljun et al. (2015), is utilized to calculate the vegetation fraction for each point in the data record.
387 Atmospheric boundary layer heights for input into the FFP come from ERA5 reanalysis (Hersbach et al.,
388 2023). Imagery from Google Earth and ArcGIS Pro software is used to visually select areas covered with
389 the vegetation of interest. Areas with the vegetation type of interest are assigned a value of one, while
390 other areas are assigned a value of zero. For all half hours during which the required input data are
391 available, the FFP climatology function simulates footprints at a 1 m grid spacing for a 501 m by 501 m
392 domain. The site map distinguishing landcover types and the footprint estimate is multiplied to obtain a
393 gridded map representing only the footprint attributable to the vegetation of interest. For every possible
394 half hour, two values are computed using the predicted footprints: a value representing the footprint
395 attributable to the vegetation of interest and a value for the total footprint. The former is calculated by
396 summing over the footprint attributable to the vegetation of interest, and the latter by summing the
397 footprint over the entire domain. The ratio of these values represents the fraction of the footprint
398 attributable to the vegetation of interest.

399
400 The agricultural EC measurements have been used to evaluate the background conditions for the city.
401 Murphy et al. (2025) evaluated the accuracy and precision of a simple carbon flux model used to describe
402 ecosystem CO₂ fluxes surrounding the city. Ongoing work is evaluating the latent and sensible heat fluxes
403 simulated by numerical weather prediction (NWP) models. These models are necessary for conducting
404 urban climate and GHG inversion studies.

405 406 **2.6 Turfgrass Sites**

407
408 Turfgrass is a common urban land cover (Milesi et al., 2005). Only a handful of towers have previously
409 been deployed to measure turfgrass lawns (i.e., mixed species low-stature vegetation often artificially
410 managed through irrigation, fertilization, and/or mowing) (Ng et al., 2015; Pahari et al., 2018; Pérez-Ruiz
411 et al., 2020; Peters and McFadden, 2012) despite these lawns being an abundant vegetative community in
412 urban areas (Horne et al., 2025). We deployed two flux towers (US-INa and US-INb) to monitor turfgrass
413 lawns. The two INFLUX turfgrass towers captured different levels of management intensity. US-INa
414 measured fluxes over a cemetery lawn (Fig. 6) with lower intensity management (i.e., infrequent mowing,
415 no fertilization, and no irrigation), and US-INb measured fluxes over a golf course (i.e., frequent mowing,
416 fertilization, and irrigation). These towers were of low stature and sited to minimize contributions to the
417 flux footprint from anything other than turfgrass. We have used the CO₂ flux data from these two turfgrass
418 towers to evaluate the Vegetation Photosynthesis and Respiration Model (VPRM) performance at
419 reproducing seasonal turfgrass fluxes, finding that these lawns require a unique representation in the
420 VPRM (Horne et al., 2025).



421
 422 **Figure 6.** The average winter (DJF) (a) and summer (JJA) (b) diel cycle of latent heat (LE), sensible heat
 423 (H), and CO₂ fluxes for US-INa (cemetery lawn). Data for averaging are taken from the periods over the
 424 site deployment (Aug 2017 – April 2019). The dashed and dashed-dot horizontal lines indicate zero
 425 crossings for the CO₂ or sensible and latent heat flux, respectively.

426

427 2.7 Heterogeneous Footprint (Mixed) Urban Flux Towers

428

429 Three communications towers with EC instrumentation at 30 to 43 m AGL were instrumented to measure
 430 fluxes from the complex, mixed land cover typical of urban environments. These higher-altitude
 431 measurements are necessary to measure fluxes above the trees and buildings commonly found throughout
 432 the metropolitan area. As mentioned, these towers host flux instrumentation and mole fraction
 433 measurements that are part of the INFLUX urban GHG testbed monitoring network (Miles et al., 2017a;
 434 Davis et al., 2017). In addition, publicly available high-resolution data, although not included here, are
 435 available and can complement specific investigations, aiding users in interpreting measurements.
 436 Footprint climatologies generated using the Kljun et al. (2015) FFP model for the INFLUX mixed urban
 437 flux towers are shown in Figs. 7. We include footprint climatologies for these sites alone to show the level
 438 of heterogeneity at each site and the estimated area measured by these towers. These footprint
 439 climatologies guide our characterization of the regions sampled by these towers. We describe broad
 440 characteristics of the urban landscapes in their flux footprints following the example of the Urban-
 441 PLUMBER project (<https://urban-plumber.github.io/>, Lipson et al., 2022). Table 4 provides metadata for
 442 the area surrounding the three heterogeneous urban flux towers (US-INc, US-INf, US-ING). In Table 4,
 443 values for roughness length (z_0) and displacement height (z_d) are provided. These length scales are
 444 simultaneously fitted using the logarithmic wind profile and isolating measurement periods during near-
 445 neutral conditions ($|z/L| < 0.05$, where z is the height of the EC measurement and L is the measured
 446 Obukhov length), where the tower frame does not impact the measurement. These provided z_d and z_0
 447 values serve as a reasonable first-order estimate for use in a flux footprint model. It should be noted that
 448

449

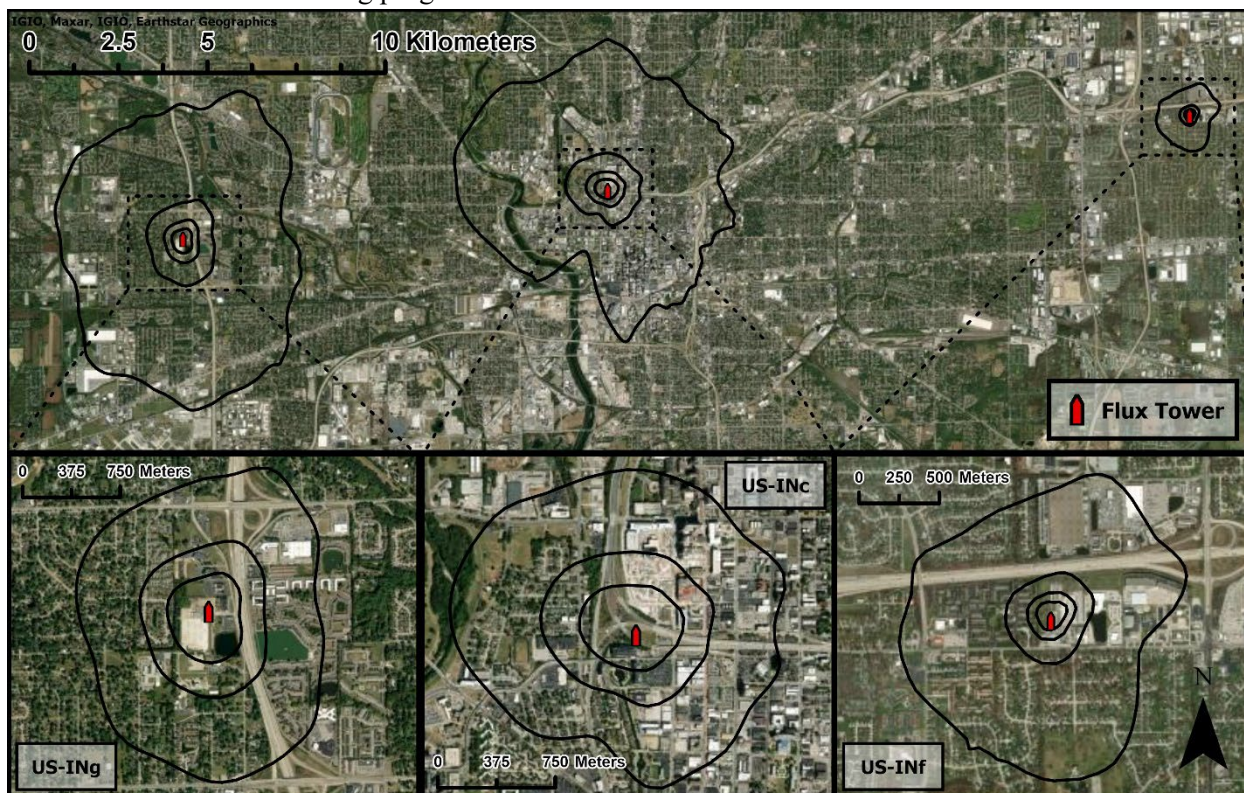
Table 4. Metadata for the surrounding land cover at the three heterogeneous flux towers. We include
 450 values of roughness length (z_0) and displacement height (z_d) for each of the towers. The domain is 4 km²
 451 centered around the respective tower and separated into quadrants NE [0-90°), SE [90-180°), SW [180-
 452 270°), and NW [270-360°) to capture heterogeneity surrounding the tower. Data for percent impervious

453 and canopy fractions come from the National Land Cover Database (NLCD) using data for 2021 (US-INc
 454 and US-INg) and 2013 (US-INf) (doi.org/10.5066/P9JZ7AO3). LiDAR data used to estimate roughness
 455 elements (RE) (buildings and trees $\geq 2\text{m}$) characteristics comes from the 2016 Indiana Statewide 3DEP
 456 LiDAR Data Products for Marion County (USDA, 2016). Roughness element density is the ratio of
 457 surface area occupied by REs to total surface area (i.e., planar area index).

Site	Quadrant	Local Climate Zone (LCZ)	Percent impervious (%)	Percent tree canopy cover (%)	Planar density ($\text{m}^2 \text{m}^{-2}$)	Mean RE height (m)	RE standard deviation (m)	Maximum RE height (m)
US-INc (43 m AGL)	NE	LCZ 8 (Large low-rise)	86	1	0.29	10.6	8.9	53
z_0 : 0.33 m	SE	LCZ 8 (Large low-rise)	85	2	0.32	9.4	8.7	57
z_d : 2 m	SW	LCZ 6 (Open low-rise)	69	5	0.33	6.9	5.2	36
	NW	LCZ 6 (Open low-rise)	58	6	0.23	5.8	3.7	25
US-INf (30 m AGL)	NE	LCZ 8 _{Bc} (Large low-rise with scattered trees)	67	4	0.27	6.1	2.7	30
z_0 : 0.17 m	SE	LCZ 6 (Open low-rise)	41	12	0.31	5.1	2.4	25
z_d : 4 m	SW	LCZ 6 (Open low-rise)	41	14	0.43	5.2	2.4	31
	NW	LCZ 6 (Open low-rise)	49	11	0.35	5	2.1	23
US-INg (41 m AGL)	NE	LCZ 8 _B (Large low-rise with scattered trees)	64	4	0.19	5.4	2.1	25
z_0 : 0.11 m	SE	LCZ 6 (Open low-rise)	50	6	0.22	5.4	2.2	22
z_d : 1.5 m	SW	LCZ 6 (Open low-rise)	35	12	0.33	5.4	2.6	34
	NW	LCZ 6 (Open low-rise)	42	15	0.33	4.9	2.2	22

458
 459 data from these towers have been employed in multiple previous studies. Wu et al. (2022) demonstrated a
 460 method of disaggregation using INFLUX EC data and mole fraction measurement profiles available at the
 461 three INFLUX mixed urban flux towers (Richardson et al., 2017; Miles et al., 2017a), as well as tracer

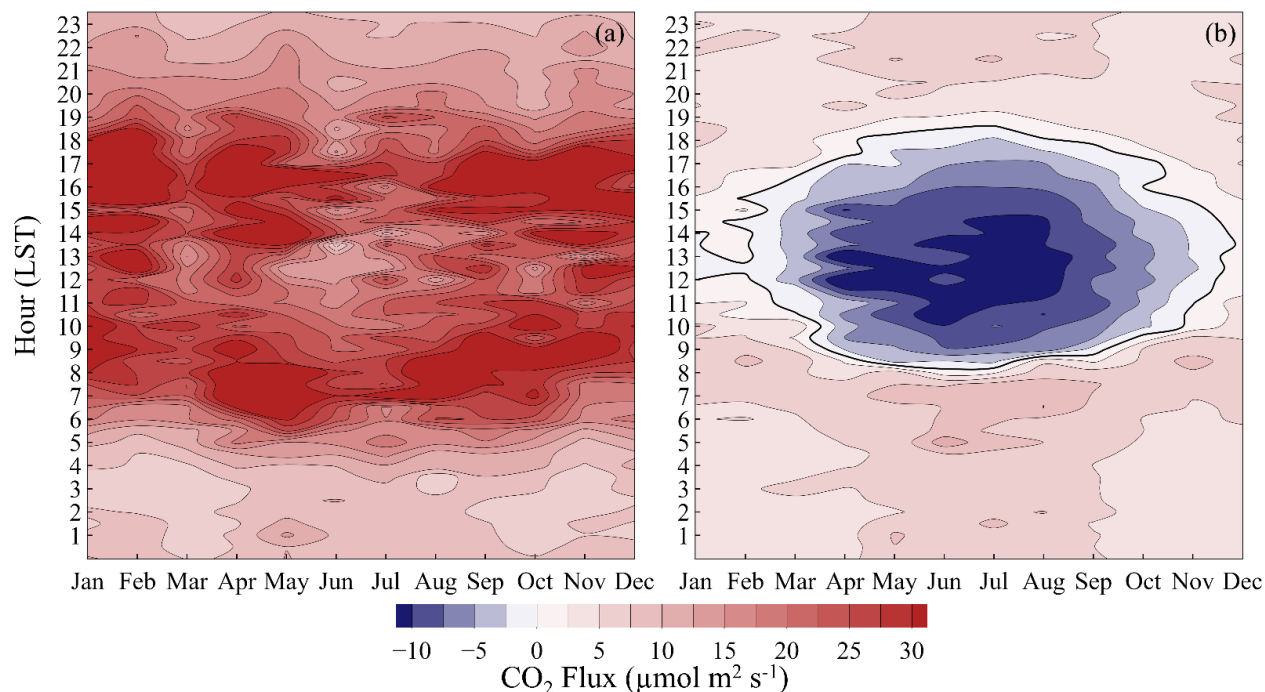
462 ratio methods. This methodology estimates the fossil fuel component of the CO₂ flux by combining
 463 carbon monoxide (CO) flux estimates with measurements of the CO to CO₂ flux ratio from fossil fuel
 464 combustion (Turnbull et al., 2015). The biogenic CO₂ flux is then determined by subtracting the fossil
 465 fuel flux from the total CO₂ flux measured via EC. Vogel et al. (2024) applied this methodology to the
 466 flux record from US-INg to study changes in emissions caused by the COVID-19 lockdown. Both Wu et
 467 al. (2022) and Vogel et al. (2024) employed flux footprint and tracer decomposition methods in
 468 conjunction to compare the EC measurements with the Hestia urban emissions inventory (Gurney et al.,
 469 2012). Kenion et al. (2024) used US-INc EC flux data to demonstrate our ability to infer local-scale urban
 470 GHG fluxes using flux-gradient and flux-variance methods. These approaches can be applied to mole
 471 fraction measurement sites that are relatively abundant across the NIST urban test beds and other urban
 472 GHG mole fraction monitoring programs.



473 **Figure 7.** Flux footprint climatologies for all three heterogeneous urban flux towers are shown. Footprint
 474 climatologies are created using the Kljun et al. (2015) flux footprint prediction (FFP) model and available
 475 data from 2022 (US-INc and US-INg) or 2013 (US-INF). Boundary layer height data for FFP are provided
 476 by ERA5 reanalysis. The outermost climatology boundary represents 90% of the area, and extents moving
 477 towards the respective tower represent a 20% decrease in climatological area (i.e., 70%, 50%, 30%).
 478 Wind directions impacted by the building wake (Fig. 2) at US-INc are removed. Zoomed-in maps of the
 479 area around each tower are provided, with their extent shown by the dashed outlines on the upper plot.
 480 Service layer credits go to Earthstar Geographics, IGIO, and Maxar.

482
 483 Two mixed urban flux towers, US-INF and US-INg, can each be interpreted as two distinct flux tower
 484 sites. We describe these differences in terms of building and vegetation cover (Table 4) and local climate
 485 zones (LCZ) (Stewart and Oke, 2012). The EC instruments at US-INg, for example, are set between a
 486 highway (LCZ E – Bare rock or paved) and commercial buildings (LCZ 8_B – Large low-rise with

487 scattered trees) to the east and a forested residential neighborhood (LCZ 6 - Open low-rise) to the west.
 488 The two sectors exhibit dissimilar diel patterns of CO₂ fluxes (Fig. 8). To the west, we observe a
 489 photosynthetic drawdown from the suburban forest during the growing season. To the east, we can
 490 observe two distinct peaks in net emissions, corresponding to morning and evening rush-hour traffic
 491 (Vogel et al., 2024). Similarly, the footprint at US-INf is roughly divided into northern and southern
 492 sectors (Table 4), with highway and commercial areas to the north and residences to the south. Multiple
 493 INFLUX studies (Vogel et al., 2024; Kenion et al., 2024; Wu et al., 2022) have shown that the results are
 494 highly interpretable using this simple wind direction interpretation.



495
 496 **Figure 8.** Isopleths of measured CO₂ flux at US-INg (April 2019 - January 2023) as a function of time of
 497 year (x-axis) and time of day (y-axis) for a) easterly wind directions (0 - 180°] and b) westerly wind
 498 directions (180 - 360°]. Positive values indicate net emissions of CO₂; negative values indicate a net
 499 uptake of CO₂.

500 We have not divided the flux data from US-INf and US-INg into two distinct records, nor have we posted
 501 flux footprint data sets to accompany each flux tower. However, the flux tower records contain all the
 502 data needed to subdivide the datasets and produce flux footprints, except for the atmospheric boundary
 503 layer height, which can be obtained from reanalysis products such as ERA5 (Hersbach et al., 2023). We
 504 note that urban systems frequently violate the assumptions implicit in the surface layer similarity theory
 505 and, consequently, the current flux footprint models (e.g., homogeneous turbulence forcing within the
 506 flux footprint). We, along with others, such as Feigenwinter et al. (2012), argue that existing footprint
 507 models (e.g., Kljun et al., 2015) remain quite helpful in interpreting these datasets. However, more
 508 research into the sensitivity of these models to complex urban systems is warranted.

509 3 Data availability

510

511 Unprocessed 10Hz data and processed INFLUX data are available on Penn State Data Commons (Table
512 5). This version contains all the processed data with flagging, but no data has been removed based on
513 flagging. This processed data also included a metadata file describing the naming convention of variables
514 and flagging. Data from all agricultural sites includes calculated fractional coverage and data collected
515 using the Arable sensors on-site.
516

517 **Table 5.** Citations for each INFLUX tower. The raw data collected directly from the instruments, a
518 processed version of the data available on Ameriflux, and a processed version with no flagged data
519 removed are available through Penn State Data Commons.

Site	10Hz Data/full processed dataset	Ameriflux
US-INa	Richardson et al. (2023a) - https://doi.org/10.26208/CJTC-KS26	Davis (2023a) - https://doi.org/10.17190/AMF/2001300
	Horne et al. (2025b) - https://doi.org/10.26208/BV87-RP98	
US-INb	Richardson et al. (2023a) - https://doi.org/10.26208/CJTC-KS26	Davis (2023b) - https://doi.org/10.17190/AMF/2001301
	Horne et al. (2025b) - https://doi.org/10.26208/BV87-RP98	
US-INc	Richardson et al. (2023b) - https://doi.org/10.26208/fsy8-h855	Davis (2023c) - https://doi.org/10.17190/AMF/1987603
	Horne et al. (2025c) - https://doi.org/10.26208/E8CE-ZH47	
US-INd	Richardson et al. (2023c) - https://doi.org/10.26208/2NT2-RS82	Davis (2023d) - https://doi.org/10.17190/AMF/2001302
	Horne et al. (2025d) - https://doi.org/10.26208/900V-YJ22	
US-INe	Richardson et al. (2023c) - https://doi.org/10.26208/2NT2-RS82	Davis (2023e) - https://doi.org/10.17190/AMF/2001303
	Horne et al. (2025d) - https://doi.org/10.26208/900V-YJ22	
US-INF	Sarmiento and Davis (2017) - https://doi.org/10.17190/AMF/2001304	Davis (2023f) - https://doi.org/10.17190/AMF/2001304
	Richardson et al. (2023b) - https://doi.org/10.26208/fsy8-h855	
US-ING	Horne et al. (2025c) - https://doi.org/10.26208/E8CE-ZH47	Davis (2023g) - https://doi.org/10.17190/AMF/2001305
	Richardson et al. (2023c) - https://doi.org/10.26208/2NT2-RS82	
US-INi	Horne et al. (2025d) - https://doi.org/10.26208/900V-YJ22	Davis (2023h) - https://doi.org/10.17190/AMF/2001306
	Richardson et al. (2023c) - https://doi.org/10.26208/2NT2-RS82	
US-INj	Richardson et al. (2023c) - https://doi.org/10.26208/2NT2-RS82	Davis (2023i) - https://doi.org/10.17190/AMF/2001307

	Horne et al. (2025d) - https://doi.org/10.26208/900V-YJ22	
	Richardson et al. (2023c) - https://doi.org/10.26208/2NT2-RS82	
US-INn	Horne et al. (2025d) - https://doi.org/10.26208/900V-YJ22	Davis (2023j) - https://doi.org/10.17190/AMF/2001308
	Richardson et al. (2023c) - https://doi.org/10.26208/2NT2-RS82	
US-INp	Horne et al. (2025d) - https://doi.org/10.26208/900V-YJ22	Davis (2023k) - https://doi.org/10.17190/AMF/2001309

520
521 In addition, all INFLUX EC datasets are available through the Ameriflux network
522 (<https://ameriflux.lbl.gov/>, Table 5). As of May 2025, the operation of all INFLUX flux towers has
523 concluded. Data collected in 2025 at US-INg and US-INc sites will be processed, updated, and made
524 available through all datasets in Table 5.

525
526 These flux measurements were a component of a broader research effort, the Indianapolis Flux
527 Experiment (INFLUX). Multiple additional measurements and model data sets exist, creating a more
528 complete experimental data set to assess urban greenhouse gases in Indianapolis, IN. These include mole
529 fraction measurements (Miles et al., 2017b), flask measurements
530 (<https://gml.noaa.gov/dv/site/?stacode=INX>), Doppler lidar measurements
531 (<https://csl.noaa.gov/projects/influx/>), anthropogenic emissions inventories (Gurney et al., 2018), aircraft
532 measurements (<https://influx.psu.edu/influx/data/flight/>), VPRM simulations (Horne and Davis, 2024;
533 Murphy et al., 2024), and Weather Research and Forecast (WRF) Reanalysis (Deng et al., 2020), which
534 are not described in detail here. For more information concerning the INFLUX Project and the data
535 collected, please visit <https://influx.psu.edu>. Most of these complementary data sets can be found at Penn
536 State’s Data Commons.

537 4 Conclusions

538
539 The INFLUX EC network has become a vital component of the multivariate INFLUX data set.
540 Micrometeorological methods like EC can bridge the gap between land surface modeling and atmospheric
541 inverse methods used to quantify urban GHG fluxes. The INFLUX EC flux data expands the growing
542 database of urban flux measurements. Data representative of the range of land-atmosphere fluxes
543 encountered in this region was obtained by deploying multiple sites representative of the land cover of the
544 city and its surroundings. We hope the data availability will support cross-collaboration between projects
545 involving urban environments.

546
547 **Author contributions.** NM, SR, and KD conceived and coordinated the INFLUX project. KD
548 conceptualized the EC flux measurement strategies for INFLUX. SR and NM installed the
549 instrumentation, and SR, NM, and BA worked on maintaining the currently deployed instruments. BJH
550 oversaw the development and implementation of the data acquisition and monitoring system, and BJH
551 and JH collaborated to create it. BA, HK, SM, and JH oversee data processing and quality control. JH led

552 the writing of this document, and all authors contributed to its editing and review. SM and JH helped
553 create footprint climatologies for heterogeneous urban towers.

554

555 **Competing interests.** The authors declare that they have no conflict of interest.

556

557 **Acknowledgements.**

558 We thank Brady Hardiman for assistance in locating the sites for US-INa and US-INb, and the Crown Hill
559 Cemetery and The Fort Golf Resort for access to these sites. We thank Hal Truax, Dave Rhoads, and
560 Andy Mohr for allowing us to deploy flux towers on their property. We thank Daniel Sarmiento for
561 leading the instrumentation and data acquisition from US-INf's EC flux measurements.

562

563 **Financial support.**

564 This work was supported by the US National Institute of Standards and Technology's urban GHG testbeds
565 program, award numbers 70NANB10H245, 70NANB23H188, 70NANB19H128, and 70NANB15H336.
566 HK was partly supported by Penn State's Institute of Energy and the Environment.

567 **References**

568 Aubinet, M., Vesala Timo, and Papale, D.: Eddy Covariance, edited by: Aubinet, M., Vesala, T., and
569 Papale, D., Springer Netherlands, Dordrecht, 0–438 pp., 2012.

570 Baldocchi, D., Falge, E., Gu, L., Olson, R., Hollinger, D., Running, S., Anthoni, P., Bernhofer, C., Davis,
571 K., Evans, R., Fuentes, J., Goldstein, A., Katul, G., Law, B., Lee, X., Malhi, Y., Meyers, T., Munger, W.,
572 Oechel, W., Paw, K. T., Pilegaard, K., Schmid, H. P., Valentini, R., Verma, S., Vesala, T., Wilson, K., and
573 Wofsy, S.: FLUXNET: A New Tool to Study the Temporal and Spatial Variability of Ecosystem–Scale
574 Carbon Dioxide, Water Vapor, and Energy Flux Densities, *Bull Am Meteorol Soc*, 82, 2415–2434,
575 [https://doi.org/10.1175/1520-0477\(2001\)082<2415:FANTTS>2.3.CO;2](https://doi.org/10.1175/1520-0477(2001)082<2415:FANTTS>2.3.CO;2), 2001.

576 Barr, A.G., Richardson, A.D., Hollinger, D.Y., Papale, D., Arain, M.A., Black T.A., Bohrer, G., Dragoni,
577 D., Fischer, M.L., Gu, L., Law, B.E., Margolis, H.A., McCaughey J.H., Munger J.W., Oechel, W.,
578 Schaeffer, K.: Use of change-point detection for friction–velocity threshold evaluation in eddy-covariance
579 studies, *Agricultural and Forest Meteorology*, 171–172, 31–45,
580 <https://doi.org/10.1016/j.agrformet.2012.11.023>, 2013.

581 Biraud, S., Chen, J., Christen, A., Davis, K., Lin, J., McFadden, J., Miller, C., Nemitz, E., Schade, G.,
582 Stagakis, S., Turnbull, J., and Vogt, T.: Eddy Covariance Measurements in Urban Environments: White
583 paper prepared by the AmeriFlux Urban Fluxes ad hoc committee, 2021.

584 Bou-Zeid, E., Anderson, W., Katul, G. G., and Mahrt, L.: The Persistent Challenge of Surface
585 Heterogeneity in Boundary-Layer Meteorology: A Review, *Boundary Layer Meteorol*, 177, 227–245,
586 <https://doi.org/10.1007/s10546-020-00551-8>, 2020.

587 Burba, G.: Eddy Covariance Method for Scientific, Industrial, Agricultural, and Regulatory Applications;
588 a field book on measuring ecosystem gas exchange and areal emission rates, LI-COR Biosciences,
589 Lincoln, Nebraska, xii–331 pp., 2013.

590 Butterworth, B.J., Desai, A.R., Metzger, S., Townsend, P.A., Schwartz, M.D., Petty, G.W., Mauder,
591 M., Vogelmann, H., Andresen, C.G., Augustine, T.J., Bertram, T.H., Brown, W.O.J., Buban, M.,
592 Cleary, P., Durden, D.J., Florian, C.R., Ruiz, E.G., Iglinski, T.J., Kruger, E.L., Lantz, K., Lee, T.R.,
593 Meyers, T.P., Mineau, J.K., Olson, E.R., Oncley, S.P., Paleri, S., Pertzborn, R.A., Pettersen, C.,
594 Plummer, D.M., Riihimaki, L., Sedlar, J., Smith, E.N., Speidel, J., Stoy, P.C., Sühning, M., Thom,
595 J.E., Turner, D.D., Vermeuel, M.P., Wagner, T.J., Wang, Z., Wanner, L., White, L.D., Wilczak,
596 J.M.M., Wright, D.B., and Zheng, T.: Connecting Land-Atmosphere Interactions to Surface
597 Heterogeneity in CHEESEHEAD19, *Bulletin of the American Meteorological Society*, 102(2), E421-
598 E445, doi:[10.1175/BAMS-D-19-0346.1](https://doi.org/10.1175/BAMS-D-19-0346.1), 2021.

599 Chu, H., Luo, X., Ouyang, Z., Chan, W. S., Dengel, S., Biraud, S. C., Torn, M. S., Metzger, S., Kumar, J.,
600 Arain, M. A., Arkebauer, T. J., Baldocchi, D., Bernacchi, C., Billesbach, D., Black, T. A., Blanken, P. D.,
601 Bohrer, G., Bracho, R., Brown, S., Brunsell, N. A., Chen, J., Chen, X., Clark, K., Desai, A. R., Duman, T.,
602 Durden, D., Fares, S., Forbrich, I., Gamon, J. A., Gough, C. M., Griffis, T., Helbig, M., Hollinger, D.,
603 Humphreys, E., Ikawa, H., Iwata, H., Ju, Y., Knowles, J. F., Knox, S. H., Kobayashi, H., Kolb, T., Law,
604 B., Lee, X., Litvak, M., Liu, H., Munger, J. W., Noormets, A., Novick, K., Oberbauer, S. F., Oechel, W.,
605 Oikawa, P., Papuga, S. A., Pendall, E., Prajapati, P., Prueger, J., Quinton, W. L., Richardson, A. D.,
606 Russell, E. S., Scott, R. L., Starr, G., Staebler, R., Stoy, P. C., Stuart-Haëntjens, E., Sonntag, O.,
607 Sullivan, R. C., Suyker, A., Ueyama, M., Vargas, R., Wood, J. D., and Zona, D.: Representativeness of
608 Eddy-Covariance flux footprints for areas surrounding AmeriFlux sites, *Agric For Meteorol*, 301–302,
609 <https://doi.org/10.1016/j.agrformet.2021.108350>, 2021.

610 Crawford, B. and Christen, A.: Spatial source attribution of measured urban eddy covariance CO₂ fluxes,
611 *Theor Appl Climatol*, 119, 733–755, <https://doi.org/10.1007/s00704-014-1124-0>, 2015.

612 Davis, K. J., Deng, A., Lauvaux, T., Miles, N. L., Richardson, S. J., Sarmiento, D. P., Gurney, K. R.,
613 Hardesty, R. M., Bonin, T. A., Brewer, W. A., Lamb, B. K., Shepson, P. B., Harvey, R. M., Cambaliza, M.
614 O., Sweeney, C., Turnbull, J. C., Whetstone, J., and Karion, A.: The Indianapolis Flux Experiment
615 (INFLUX): A test-bed for developing urban greenhouse gas emission measurements, *Elementa: Science*
616 *of the Anthropocene*, 5, <https://doi.org/10.1525/elementa.188>, 2017.

617 Davis, K.J., P.S. Bakwin, B.W. Berger, C. Yi, C. Zhao, R.M. Teclaw and J.G. Isebrands.: The annual cycle
618 of CO₂ and H₂O exchange over a northern mixed forest as observed from a very tall tower. *Global Change*
619 *Biology*, 9, 1278-1293, <https://doi.org/10.1046/j.1365-2486.2003.00672.x>, 2003.

620 Davis K. J. AmeriFlux BASE US-INa INFLUX - Cemetery Turfgrass Tower, Ver. 1-5, AmeriFlux AMP,
621 (data set), <https://doi.org/10.17190/AMF/2001300>, 2023a.

622 Davis K. J. AmeriFlux BASE US-INb INFLUX - Golf Course, Ver. 1-5, AmeriFlux AMP, (data set),
623 <https://doi.org/10.17190/AMF/2001301>, 2023b.

624 Davis K. J. AmeriFlux BASE US-INc INFLUX - Downtown Indianapolis (Site-3), Ver. 1-5, AmeriFlux
625 AMP, (data set), <https://doi.org/10.17190/AMF/1987603>, 2023c.

626 Davis K. J. AmeriFlux BASE US-INd INFLUX - Agricultural Site East near Pittsboro, Ver. 1-5,
627 AmeriFlux AMP, (data set), <https://doi.org/10.17190/AMF/2001302>, 2023d.

628 Davis K. J. AmeriFlux BASE US-INe INFLUX - Agricultural Site West near Pittsboro, Ver. 1-5,
629 AmeriFlux AMP, (data set), <https://doi.org/10.17190/AMF/2001303>, 2023e.

630 Davis K. J. AmeriFlux BASE US-INf INFLUX - East 21st St (Site 2), Ver. 1-5, AmeriFlux AMP, (data
631 set), <https://doi.org/10.17190/AMF/2001304>, 2023f.

632 Davis K. J. AmeriFlux BASE US-INg INFLUX - Wayne Twp Comm (Site-7), Ver. 1-5, AmeriFlux AMP,
633 (data set), <https://doi.org/10.17190/AMF/2001305>, 2023g.

634 Davis K. J. AmeriFlux BASE US-INi INFLUX - Agricultural Site East of Indianapolis (Site-9a), Ver. 1-5,
635 AmeriFlux AMP, (data set), <https://doi.org/10.17190/AMF/2001306>, 2023h.

636 Davis K. J. AmeriFlux BASE US-INj INFLUX - Agricultural Site East of Indianapolis (Site-9b), Ver. 1-5,
637 AmeriFlux AMP, (data set), <https://doi.org/10.17190/AMF/2001307>, 2023i.

638 Davis K. J. AmeriFlux BASE US-INn INFLUX - Agricultural Site West of Indianapolis (Site-14a), Ver. 1-
639 5, AmeriFlux AMP, (data set), <https://doi.org/10.17190/AMF/2001308>, 2023j.

640 Davis K. J. AmeriFlux BASE US-INn INFLUX - Agricultural Site West of Indianapolis (Site-14b), Ver.
641 1-5, AmeriFlux AMP, (data set), <https://doi.org/10.17190/AMF/2001309>, 2023k.

642 Davis, K., Zaitchik, B., Asa-Awuku, A., Bou-Zeid, E., Baidar, S., Boxe, C., Brewer, W. A., Chiao, S.,
643 Damoah, R., Decarlo, P., Demoz, B., Dickerson, R., Giometto, M., Gonzalez-Cruz, J., Jensen, M., Kuang,
644 C., Lamer, K., Li, X., Lombardo, K., Miles, N., Niyogi, D., Pan, Y., Peters, J., Ramamurthy, P., Peng, W.,
645 Richardson, S., Sakai, R., Waugh, D., and Zhang, J.: Coastal-Urban-Rural Atmospheric Gradient
646 Experiment (CoURAGE) Science Plan, 1–50 pp., 2024.

647 Dennis, L.; Richardson, S.; Miles, N.; Woda, J.; Brantley, S.; Davis, K.: Measurements of Atmospheric
648 Methane Emissions from Stray Gas Migration: A Case Study from the Marcellus Shale. *ACS Earth Space*
649 *Chem*, 6, 4, 909–919, <https://doi.org/10.1021/acsearthspacechem.1c00312>, 2022.

650 Desjardins, R.L., P.H. Schuepp, J.I. MacPherson, and D.J. Buckley.: Spatial and temporal variations of the
651 fluxes of carbon dioxide and sensible and latent heat over the FIFE site. *J. Geophys. Res.* 97: 18 467–18
652 475, 1992.

653 Deng, A., Lauvaux, T., Miles, N. L., Davis, K. J., Barkley, Z. R. Meteorological fields over Indianapolis,
654 IN from the Weather Research and Forecasting model (WRF v3.5.1), Penn State DataCommons [data
655 set], <https://doi.org/10.26208/z04g-3h91>, 2020.

656 De Ridder, K.: Bulk Transfer Relations for the Roughness Sublayer, *Boundary Layer Meteorology*, 134,
657 257–267, <https://doi.org/10.1007/s10546-009-9450-y>, 2010.

658 Dragoni, D., Schmid, H. P., Wayson, C., Potters, H., Grimmond, S., and Randolph, J.: Evidence of
659 increased net ecosystem productivity associated with a longer vegetated season in a deciduous forest in
660 south-central Indiana, USA, *Glob Chang Biol*, 17, 886–897, <https://doi.org/10.1111/j.1365->
661 2486.2010.02281.x, 2011.

662 Dyer, A. J.: A review of flux-profile relationships, *Boundary Layer Meteorology*, 7, 363–372,
663 <https://doi.org/10.1007/BF00240838>, 1974.

664 Eder, F., Schmidt, M., Damian, T., Träumner, K., and Mauder, M.: Mesoscale Eddies Affect Near-Surface
665 Turbulent Exchange: Evidence from Lidar and Tower Measurements, *J Appl Meteorol Climatol*, 54, 189–
666 206, <https://doi.org/10.1175/JAMC-D-14-0140.1>, 2015a.

667 Eder, F., De Roo, F., Rotenberg, E., Yakir, D., Schmid, H. P., and Mauder, M.: Secondary circulations at a
668 solitary forest surrounded by semi-arid shrubland and their impact on eddy-covariance measurements,
669 *Agric For Meteorol*, 211–212, 115–127, <https://doi.org/10.1016/j.agrformet.2015.06.001>, 2015b.

670 European Union: Accelerating cities’ transition to net zero emissions by 2030 (NetZeroCities): Fact sheet,
671 European Commission, Grant Agreement No. 101036519, <https://doi.org/10.3030/101036519>, 2025.

672 Feigenwinter, C., Vogt, R., and Christen, A.: Eddy Covariance Measurements Over Urban Areas, in: *Eddy
673 Covariance*, Springer Netherlands, Dordrecht, 377–397, https://doi.org/10.1007/978-94-007-2351-1_16,
674 2012.

675 Foken, T.: *Micrometeorology*, Carmen J. Nappo., Springer, 2008.

676 Foken, Th. and Wichura, B.: Tools for quality assessment of surface-based flux measurements, *Agric For
677 Meteorol*, 78, 83–105, [https://doi.org/10.1016/0168-1923\(95\)02248-1](https://doi.org/10.1016/0168-1923(95)02248-1), 1996.

678 Gurney KR, Razlivanov I, Song Y, Zhou Y, Benes B, Abdul-Massih M.: Quantification of Fossil Fuel CO
679 ₂ Emissions on the Building/Street Scale for a Large U.S. City. *Environ Sci Technol* 46(21): 12194–
680 12202. doi: 10.1021/es3011282, 2012.

681 Gurney, K. R., Patarasuk R., Liang, J., Yuyu, Z., O’Keeffe, D., Hutchins, M., Huang, J., Song, Y., Rao, P.,
682 Wong, T. M., Whetstone, J. R., Hestia Fossil Fuel Carbon Dioxide Emissions for Indianapolis, Indiana,
683 National Institute of Standards and Technology, NIST Public Data Repository [data set],
684 <https://doi.org/10.18434/T4/1503341>, 2018.

685 Hersbach, H., Bell, B., Berrisford, P., Biavati, G., Horányi, A., Muñoz Sabater, J., Nicolas, J., Peubey, C.,
686 Radu, R., Rozum, I., Schepers, D., Simmons, A., Soci, C., Dee, D., Thépaut, J.-N., ERA5 hourly data on
687 single levels from 1940 to present. Copernicus Climate Change Service (C3S) Climate Data Store (CDS)
688 [data set], <https://doi.org/10.24381/cds.adbb2d47>, 2023.

689 Horne, J. P., Davis, K. J. Vegetation Photosynthesis and Respiration Model (VPRM) run for 2019 over
690 Indianapolis, IN, using a turfgrass PFT, Penn State DataCommons [data set],
691 <https://doi.org/10.26208/zs32-5n02>, 2024.

692 Horne, J. P., Jin, C., Miles, N. L., Richardson, S. J., Murphy, S. L., Wu, K., and Davis, K. J.: The Impact
693 of Turfgrass on Urban Carbon Dioxide Fluxes in Indianapolis, Indiana, USA,
694 <https://doi.org/10.1029/2024JG008477>, 2025a.

695 Horne, J., K. J. Davis, S. J. Richardson, N. L. Miles, S. Murphy, B. J. Haupt, H. Kenion, and B.
696 Ahlswede. Turfgrass INFLUX Eddy Covariance Towers - Processed 30-Minute Data. Penn State Data
697 Commons [data set], <https://doi.org/10.26208/BV87-RP98>, 2025b.

698 Horne, J., K. J. Davis, S. J. Richardson, N. L. Miles, S. Murphy, B. J. Haupt, H. Kenion, and B.
699 Ahlswede. Mixed Urban INFLUX Eddy Covariance Towers - Processed 30-Minute Data. Penn State Data
700 Commons [data set], <https://doi.org/10.26208/BV87-RP98>, 2025c.

701 Horne, J., K. J. Davis, S. J. Richardson, N. L. Miles, S. Murphy, B. J. Haupt, H. Kenion, and B.
702 Ahlswede. Agricultural INFLUX Eddy Covariance Towers - Processed 30-Minute Data. Penn State Data
703 Commons [data set], <https://doi.org/10.26208/900V-YJ22>, 2025d.

704 Horst, T.W., and J.C. Weil.: Footprint estimation for scalar flux measurements in the atmospheric surface
705 layer. *Boundary Layer Meteorol.* **59**: 279–296, 1992.

706 Järvi, L., Rannik, U., Kokkonen, T. V., Kurppa, M., Karppinen, A., Kouznetsov, R. D., Rantala, P., Vesala,
707 T., and Wood, C. R.: Uncertainty of eddy covariance flux measurements over an urban area based on two
708 towers, *Atmos Meas Tech*, **11**, 5421–5438, <https://doi.org/10.5194/amt-11-5421-2018>, 2018.

709 Jongen, H. J., Steeneveld, G. J., Beringer, J., Christen, A., Chrysoulakis, N., Fortuniak, K., Hong, J.,
710 Hong, J. W., Jacobs, C. M. J., Järvi, L., Meier, F., Pawlak, W., Roth, M., Theeuwes, N. E., Velasco, E.,
711 Vogt, R., and Teuling, A. J.: Urban Water Storage Capacity Inferred From Observed Evapotranspiration
712 Recession, *Geophys Res Lett*, **49**, <https://doi.org/10.1029/2021GL096069>, 2022.

713 Kaimal, J. C., Wyngaard, J. C., Izumi, Y., and Coté, O. R.: Spectral characteristics of surface-layer
714 turbulence, *Quarterly Journal of the Royal Meteorological Society*, **98**, 563–589,
715 <https://doi.org/10.1002/qj.49709841707>, 1972.

716 Kang, S., K.J. Davis and M.A. LeMone.: Observations of the ABL structures over a heterogeneous land
717 surface during IHOP_2002. *J. Hydrometeorology*, **8**, 221–244, DOI: 10.1175/JHM567.1, 2007.

718 Karion, A., Ghosh, S., Lopez-Coto, I., Mueller, K., Gourdji, S., Pitt, J., and Whetstone, J.: Methane
719 Emissions Show Recent Decline but Strong Seasonality in Two US Northeastern Cities, *Environ Sci*
720 *Technol*, **57**, 19565–19574, <https://doi.org/10.1021/acs.est.3c05050>, 2023.

721 Kenion, H. C., Davis, K. J., Miles, N. L., Monteiro, V. C., Richardson, S. J., and Horne, J. P.: Estimation
722 of Urban Greenhouse Gas Fluxes from Mole Fraction Measurements Using Monin–Obukhov Similarity
723 Theory, *J Atmos Ocean Technol*, **41**, 833–846, <https://doi.org/10.1175/JTECH-D-23-0164.1>, 2024.

724 Kent, C. W., Lee, K., Ward, H. C., Hong, J. W., Hong, J., Gatey, D., and Grimmond, S.: Aerodynamic
725 roughness variation with vegetation: analysis in a suburban neighbourhood and a city park, *Urban*
726 *Ecosyst*, **21**, 227–243, <https://doi.org/10.1007/s11252-017-0710-1>, 2018.

727 Kljun, N., Calanca, P., Rotach, M. W., and Schmid, H. P.: A simple two-dimensional parameterisation for
728 Flux Footprint Prediction (FFP), *Geosci Model Dev*, **8**, 3695–3713, [https://doi.org/10.5194/gmd-8-3695-](https://doi.org/10.5194/gmd-8-3695-2015)
729 [2015](https://doi.org/10.5194/gmd-8-3695-2015), 2015.

730 Kona, A., Bertoldi, P., Monforti-Ferrario, F., Rivas, S., and Dallemand, J.-F.: Covenant of Mayors
731 signatories leading the way towards 1.5 degree global warming pathway, *Sustain. Cities Soc.*, **41**, 568–
732 [575](https://doi.org/10.1016/j.scs.2018.05.017), <https://doi.org/10.1016/j.scs.2018.05.017>, 2018.

- 733 Kotthaus, S. and Grimmond, C. S. B.: Energy exchange in a dense urban environment – Part I: Temporal
734 variability of long-term observations in central London, *Urban Clim*, 10, 261–280,
735 <https://doi.org/10.1016/j.uclim.2013.10.002>, 2014.
- 736 Lan, C., Mauder, M., Stagakis, S., Loubet, B., D’Onofrio, C., Metzger, S., Durden, D., and Herig-
737 Coimbra, P.-H.: Intercomparison of eddy-covariance software for urban tall-tower sites, *Atmos Meas*
738 *Tech*, 17, 2649–2669, <https://doi.org/10.5194/amt-17-2649-2024>, 2024.
- 739 Lauvaux, T., Gurney, K. R., Miles, N. L., Davis, K. J., Richardson, S. J., Deng, A., Nathan, B. J., Oda, T.,
740 Wang, J. A., Hutyra, L., and Turnbull, J.: Policy-relevant assessment of urban CO₂ emissions, *Environ*
741 *Sci Technol*, 54, 10237–10245, <https://doi.org/10.1021/acs.est.0c00343>, 2020.
- 742 Lee, X. and Massman, W. J.: A Perspective on Thirty Years of the Webb, Pearman and Leuning Density
743 Corrections, *Boundary Layer Meteorol*, 139, 37–59, <https://doi.org/10.1007/s10546-010-9575-z>, 2011.
- 744 Lee, X., Massman, W., and Law, B.: *Handbook of Micrometeorology*, edited by: Lee, X., Massman, W.,
745 and Law, B., Springer Netherlands, Dordrecht, 1–250 pp., <https://doi.org/10.1007/1-4020-2265-4>, 2004.
- 746 Lipson, M., Grimmond, S., Best, M., Chow, W. T. L., Christen, A., Chrysoulakis, N., Coutts, A.,
747 Crawford, B., Earl, S., Evans, J., Fortuniak, K., Heusinkveld, B. G., Hong, J.-W., Hong, J., Järvi, L., Jo,
748 S., Kim, Y.-H., Kotthaus, S., Lee, K., Masson, V., McFadden, J. P., Michels, O., Pawlak, W., Roth, M.,
749 Sugawara, H., Tapper, N., Velasco, E., and Ward, H. C.: Harmonized gap-filled datasets from 20 urban
750 flux tower sites, *Earth Syst Sci Data*, 14, 5157–5178, <https://doi.org/10.5194/essd-14-5157-2022>, 2022.
- 751 Liu, H. Z., Feng, J. W., Järvi, L., and Vesala, T.: Four-year (2006–2009) eddy covariance measurements of
752 CO₂ flux over an urban area in Beijing, *Atmos Chem Phys*, 12, 7881–7892, [https://doi.org/10.5194/acp-](https://doi.org/10.5194/acp-12-7881-2012)
753 [12-7881-2012](https://doi.org/10.5194/acp-12-7881-2012), 2012.
- 754 Lwasa, S., K.C. Seto, X. Bai, H. Blanco, K.R. Gurney, Ş. Kılıç, O. Lucon, J. Murakami, J. Pan, A.
755 Sharifi, and Y. Yamagata: Urban Systems and Other Settlements, in: *Climate Change 2022 - Mitigation of*
756 *Climate Change*, Cambridge University Press, 861–952, <https://doi.org/10.1017/9781009157926.010>,
757 2023.
- 758 Mauder, M. and Foken, T.: *Documentation and Instruction Manual of the Eddy Covariance Software*
759 *Package TK2*, 1 pp., 2004.
- 760 Mauder, M., Foken, T., and Cuxart, J.: Surface-Energy-Balance Closure over Land: A Review, *Boundary*
761 *Layer Meteorol*, 177, 395–426, <https://doi.org/10.1007/s10546-020-00529-6>, 2020.
- 762 Menzer, O. and McFadden, J. P.: Statistical partitioning of a three-year time series of direct urban net
763 CO₂ flux measurements into biogenic and anthropogenic components, *Atmos Environ*, 170, 319–333,
764 <https://doi.org/10.1016/j.atmosenv.2017.09.049>, 2017.
- 765 Miles, N. L., Richardson, S. J., Lauvaux, T., Davis, K. J., Balashov, N. V., Deng, A., Turnbull, J. C.,
766 Sweeney, C., Gurney, K. R., Patarasuk, R., Razlivanov, I., Cambaliza, M. O. L., and Shepson, P. B.:
767 Quantification of urban atmospheric boundary layer greenhouse gas dry mole fraction enhancements in

768 the dormant season: Results from the Indianapolis Flux Experiment (INFLUX), *Elementa: Science of the*
769 *Anthropocene*, 5, <https://doi.org/10.1525/elementa.127>, 2017a.

770 Miles, N. L., Richardson, S. J., Davis, K. J., Haupt, B. J.: In-situ tower atmospheric measurements of
771 carbon dioxide, methane and carbon monoxide mole fraction for the Indianapolis Flux (INFLUX) project,
772 Indianapolis, IN, USA., Penn State DataCommons [data set], <https://doi.org/10.18113/D37G6P>, 2017b.

773 Milesi, C., Running, S. W., Elvidge, C. D., Dietz, J. B., Tuttle, B. T., and Nemani, R. R.: Mapping and
774 Modeling the Biogeochemical Cycling of Turf Grasses in the United States, *Environ Manage*, 36, 426–
775 438, <https://doi.org/10.1007/s00267-004-0316-2>, 2005.

776 Miller, J. B., Lehman, S. J., Verhulst, K. R., Miller, C. E., Duren, R. M., Yadav, V., Newman, S., and
777 Sloop, C. D.: Large and seasonally varying biospheric CO₂ fluxes in the Los Angeles megacity revealed
778 by atmospheric radiocarbon, *Proceedings of the National Academy of Sciences*, 117, 26681–26687,
779 <https://doi.org/10.1073/pnas.2005253117>, 2020.

780 Moncrieff, J. B., Massheder, J. M., de Bruin, H., Elbers, J., Friborg, T., Heusinkveld, B., Kabat, P., Scott,
781 S., Soegaard, H., and Verhoef, A.: A system to measure surface fluxes of momentum, sensible heat, water
782 vapour and carbon dioxide, *J Hydrol (Amst)*, 188–189, 589–611, [https://doi.org/10.1016/S0022-](https://doi.org/10.1016/S0022-1694(96)03194-0)
783 1694(96)03194-0, 1997.

784 Moore, C. J.: Frequency response corrections for eddy correlation systems, *Boundary Layer Meteorol*, 37,
785 17–35, <https://doi.org/10.1007/BF00122754>, 1986.

786 Murphy, S. L., Davis, K. J., Miles, N. L. Penn State Department of Meteorology Vegetation
787 Photosynthesis and Respiration Model (VPRM) runs for Indianapolis, IN, from 2012 through 2021, Penn
788 State DataCommons [data set], <https://doi.org/10.26208/zs32-5n02>, 2024.

789 Murphy, S. L., Davis, K. J., Miles, N. L., Barkley, Z. R., Deng, A., Horne, J. P., Richardson, S. J., and
790 Gourdj, S. M.: Simulating complex CO₂ background conditions for Indianapolis, IN, with a simple
791 ecosystem CO₂ flux model. *Journal of Geophysical Research: Biogeosciences*, 130, e2024JG008518.
792 <https://doi.org/10.1029/2024JG008518>, 2025.

793 Ng, B. J. L., Hutyra, L. R., Nguyen, H., Cobb, A. R., Kai, F. M., Harvey, C., and Gandois, L.: Carbon
794 fluxes from an urban tropical grassland, *Environmental Pollution*, 203, 227–234,
795 <https://doi.org/10.1016/j.envpol.2014.06.009>, 2015.

796 Nicolini, G., Antoniella, G., Carotenuto, F., Christen, A., Ciais, P., Feigenwinter, C., Gioli, B., Stagakis,
797 S., Velasco, E., Vogt, R., Ward, H. C., Barlow, J., Chrysoulakis, N., Duce, P., Graus, M., Helfter, C.,
798 Heusinkveld, B., Järvi, L., Karl, T., Marras, S., Masson, V., Matthews, B., Meier, F., Nemitz, E.,
799 Sabbatini, S., Scherer, D., Schume, H., Sirca, C., Steeneveld, G.-J., Vagnoli, C., Wang, Y., Zaldei, A.,
800 Zheng, B., and Papale, D.: Direct observations of CO₂ emission reductions due to COVID-19 lockdown
801 across European urban districts, *Science of The Total Environment*, 830, 154662,
802 <https://doi.org/10.1016/j.scitotenv.2022.154662>, 2022.

803 Novick, K.A., J.A. Biederman, A.R. Desai, M.E. Litvak, D.J.P. Moore, R.L. Scott and M.S. Torn, The
804 AmeriFlux network: A coalition of the willing, *Agricultural and Forest Meteorology*, 249, 444-456,
805 <https://doi.org/10.1016/j.agrformet.2017.10.009>, 2018.

806 Mahrt, L., D. Vickers, J. Sun.: Spatial variations of surface moisture flux from aircraft data, *Advances in*
807 *Water Resources*, 24, 9–10, 1133-1141, [https://doi.org/10.1016/S0309-1708\(01\)00045-8](https://doi.org/10.1016/S0309-1708(01)00045-8). 2001.

808 Oncley, S. P., Lenschow, D. H., Campos, T. L., Davis, K. J., and Mann, J.: Regional-scale surface flux
809 observations across the boreal forest during BOREAS, *Journal of Geophysical Research: Atmospheres*,
810 102, 29147–29154, <https://doi.org/10.1029/97JD00242>, 1997.

811 Pahari, R., Leclerc, M. Y., Zhang, G., Nahrawi, H., and Raymer, P.: Carbon dynamics of a warm season
812 turfgrass using the eddy-covariance technique, *Agric Ecosyst Environ*, 251, 11–25,
813 <https://doi.org/10.1016/j.agee.2017.09.015>, 2018.

814 Papale, D., Antoniella, G., Nicolini, G., Gioli, B., Zaldei, A., Vogt, R., Feigenwinter, C., Stagakis, S.,
815 Chrysoulakis, N., Järvi, L., Nemitz, E., Helfter, C., Barlow, J., Meier, F., Velasco, E., Christen, A., and
816 Masson, V.: Clear evidence of reduction in urban CO₂ emissions as a result of COVID-19 lockdown
817 across Europe, 2020.

818 Papale, D., Andreas, C., Davis, K., Christian, F., Beniamino Gioli, Leena, J., Bradley, M., Erik, V., and
819 Roland, V.: Eddy covariance flux observations., *GAW Report*, 275, 114–123, 2022.

820 Pastorello, G., Trotta, C., Canfora, E., Chu, H., Christianson, D., Cheah, Y. W., Poindexter, C., Chen, J.,
821 Elbashandy, A., Humphrey, M., Isaac, P., Polidori, D., Ribeca, A., van Ingen, C., Zhang, L., Amiro, B.,
822 Ammann, C., Arain, M. A., Ardö, J., Arkebauer, T., Arndt, S. K., Arriga, N., Aubinet, M., Aurela, M.,
823 Baldocchi, D., Barr, A., Beamesderfer, E., Marchesini, L. B., Bergeron, O., Beringer, J., Bernhofer, C.,
824 Berveiller, D., Billesbach, D., Black, T. A., Blanken, P. D., Bohrer, G., Boike, J., Bolstad, P. V., Bonal, D.,
825 Bonnefond, J. M., Bowling, D. R., Bracho, R., Brodeur, J., Brümmer, C., Buchmann, N., Burban, B.,
826 Burns, S. P., Buysse, P., Cale, P., Cavagna, M., Cellier, P., Chen, S., Chini, I., Christensen, T. R., Cleverly,
827 J., Collalti, A., Consalvo, C., Cook, B. D., Cook, D., Coursolle, C., Cremonese, E., Curtis, P. S.,
828 D’Andrea, E., da Rocha, H., Dai, X., Davis, K. J., De Cinti, B., de Grandcourt, A., De Ligne, A., De
829 Oliveira, R. C., Delpierre, N., Desai, A. R., Di Bella, C. M., di Tommasi, P., Dolman, H., Domingo, F.,
830 Dong, G., Dore, S., Duce, P., Dufréne, E., Dunn, A., Dušek, J., Eamus, D., Eichelmann, U., ElKhidir, H.
831 A. M., Eugster, W., Ewenz, C. M., Ewers, B., Famulari, D., Fares, S., Feigenwinter, I., Feitz, A., Fensholt,
832 R., Filippa, G., Fischer, M., Frank, J., Galvagno, M., Gharun, M., Gianelle, D., et al.: The
833 FLUXNET2015 dataset and the ONEFlux processing pipeline for eddy covariance data, *Sci Data*, 7, 225,
834 <https://doi.org/10.1038/s41597-020-0534-3>, 2020.

835 Paw U, K. T., Baldocchi, D. D., Meyers, T. P., and Wilson, K. B.: Correction Of Eddy-Covariance
836 Measurements Incorporating Both Advective Effects And Density Fluxes, *Boundary Layer Meteorol*, 97,
837 487–511, <https://doi.org/10.1023/A:1002786702909>, 2000.

838 Pawlak, W. and Fortuniak, K.: Eddy covariance measurements of the net turbulent methane flux in the
839 city centre-results of 2-year campaign in Lodz, Poland, *Atmos Chem Phys*, 16, 8281–8294,
840 <https://doi.org/10.5194/acp-16-8281-2016>, 2016.

841 Pérez-Ruiz, E. R., Vivoni, E. R., and Templeton, N. P.: Urban land cover type determines the sensitivity
842 of carbon dioxide fluxes to precipitation in Phoenix, Arizona, *PLoS One*, 15,
843 <https://doi.org/10.1371/journal.pone.0228537>, 2020.

844 Peters, E. B. and McFadden, J. P.: Continuous measurements of net CO₂ exchange by vegetation and
845 soils in a suburban landscape, *J Geophys Res Biogeosci*, 117, <https://doi.org/10.1029/2011JG001933>,
846 2012.

847 Peters, E. B., Hiller, R. V., and McFadden, J. P.: Seasonal contributions of vegetation types to suburban
848 evapotranspiration, *J Geophys Res Biogeosci*, 116, <https://doi.org/10.1029/2010JG001463>, 2011.

849 Prairie, Y. T. and Duarte, C. M.: Direct and indirect metabolic CO₂ release by humanity, *Biogeosciences*,
850 4, 215–217, <https://doi.org/10.5194/bg-4-215-2007>, 2007.

851 Raut, B. A., Muradyan, P., Pal, S., Ivans, S., Tuftedal, M., Sherman, Z., Grover, M., O'Brien, J., Jackson,
852 R., Wawrzyniak, E., Cho, A., Anderson, G., Gala, T., and Collis, S.: The Chicago Urban Flux Network
853 with Perspectives from an Eddy Covariance Workshop, *Bull Am Meteorol Soc*, 106, E1724–E1730,
854 <https://doi.org/10.1175/BAMS-D-25-0180.1>, 2025.

855 Richardson, S. J., Miles, N. L., Davis, K. J., Lauvaux, T., Martins, D. K., Turnbull, J. C., McKain, K.,
856 Sweeney, C., and Cambaliza, M. O. L.: Tower measurement network of in-situ CO₂, CH₄, and CO in
857 support of the Indianapolis FLUX (INFLUX) Experiment, *Elementa: Science of the Anthropocene*, 5,
858 <https://doi.org/10.1525/elementa.140>, 2017.

859 Richardson, S. J., Miles, N. L., Haupt, B. J., Ahlswede, B., Horne, J. P., Davis, K. J. Eddy Covariance
860 High-Frequency Data for Turfgrass and Pasture in Indianapolis, Indiana and Montgomery County,
861 Maryland (US-INa, US-INb, US-BWa, US-BWb, US-BWc), Penn State DataCommons [data set],
862 <https://doi.org/10.26208/CJTC-KS26>, 2023a.

863 Richardson, S. J., Miles, N. L., Haupt, B. J., Ahlswede, B., Horne, J. P., Davis, K. J. Eddy Covariance
864 High-Frequency Data for Agricultural Sites near Indianapolis, Indiana (US-IND, US-INE, US-INi, US-INj,
865 US-INn, US-INp), Penn State DataCommons [data set], <https://doi.org/10.26208/fsy8-h855>, 2023b.

866 Richardson, S. J., Miles, N. L., Haupt, B. J., Ahlswede, B., Horne, J. P., Davis, K. J. Eddy Covariance
867 High-Frequency Data for Urban and Suburban Sites in Indianapolis, Indiana (US-INc, US-ING), Penn
868 State DataCommons [data set], <https://doi.org/10.26208/2NT2-RS82>, 2023c.

869 Sarmiento, D. P., Davis, K. J., Deng, A., Lauvaux, T., Brewer, A., and Hardesty, M.: A comprehensive
870 assessment of land surface-atmosphere interactions in a WRF/Urban modeling system for Indianapolis,
871 IN, *Elementa: Science of the Anthropocene*, 5, <https://doi.org/10.1525/elementa.132>, 2017.

872 Sarmiento, D. P., Davis, K. J. Eddy covariance flux tower data for Indianapolis, IN (INFLUX project),
873 Penn State DataCommons [data set], <https://doi.org/10.17190/AMF/2001304>, 2017.

874 Schmid, H. P., Grimmond, S., Cropley, F., Offerle, B., and Su, H.-B.: Measurements of CO₂ and energy
875 fluxes over a mixed hardwood forest in the mid-western United States, *Agric For Meteorol*, 103, 357–
876 374, [https://doi.org/10.1016/S0168-1923\(00\)00140-4](https://doi.org/10.1016/S0168-1923(00)00140-4), 2000.

877 Schuepp, P. H., Leclerc, M. Y., MacPherson, J. I., and Desjardins, R. L.: Footprint prediction of scalar
878 fluxes from analytical solutions of the diffusion equation, *Boundary Layer Meteorol*, 50, 355–373,
879 <https://doi.org/10.1007/BF00120530>, 1990.

880 Semerjian, H. G. and Whetstone, J. R.: Urban greenhouse gas measurements :,
881 <https://doi.org/10.6028/NIST.TN.2145>, 2021.

882 Shi, Y., K. J. Davis, C. J. Duffy, X. Yu.: Development of a Coupled Land Surface Hydrologic Model and
883 Evaluation at a Critical Zone Observatory. *J. Hydrometeorol*, 14, 1401–1420, 2013.

884 Stagakis, S., Chrysoulakis, N., Spyridakis, N., Feigenwinter, C., and Vogt, R.: Eddy covariance
885 measurements and source partitioning of CO₂ emissions in an urban environment: application for
886 Heraklion, Greece, *Atmos. Environ.*, 201, 278–292, <https://doi.org/10.1016/j.atmosenv.2019.01.009>,
887 2019.

888 Stewart, I. D. and Oke, T. R.: Local climate zones for urban temperature studies, *Bull Am Meteorol Soc*,
889 93, 1879–1900, <https://doi.org/10.1175/BAMS-D-11-00019.1>, 2012.

890 Sun, L., Chen, J., Li, Q., and Huang, D.: Dramatic uneven urbanization of large cities throughout the
891 world in recent decades, *Nat Commun*, 11, 5366, <https://doi.org/10.1038/s41467-020-19158-1>, 2020.

892 Southwest Integrated Field Laboratory (SW-IFL): 2024 Annual Report – Addressing extreme heat and
893 associated environmental and societal stressors through resilient solutions & next-generation predictive
894 tools, DOE Award #DE-SC0023520, U.S. Department of Energy, Washington, D.C., USA, 2024

895 Turnbull, J. C., Karion, A., Davis, K. J., Lauvaux, T., Miles, N. L., Richardson, S. J., Sweeney, C.,
896 McKain, K., Lehman, S. J., Gurney, K. R., Patarasuk, R., Liang, J., Shepson, P. B., Heimburger, A.,
897 Harvey, R., and Whetstone, J.: Synthesis of Urban CO₂ Emission Estimates from Multiple Methods from
898 the Indianapolis Flux Project (INFLUX), *Environ Sci Technol*, 53, 287–295,
899 <https://doi.org/10.1021/acs.est.8b05552>, 2019.

900 Turnbull, J. C., Curras, T., Gurney, K. R., Hilton, T. W., Mueller, K. L., Vogel, F., Yao, B., Albarus, I.,
901 Ars, S., Baidar, S., Chatterjee, A., Chen, H., Chen, J., Christen, A., Davis, K. J., Hajny, K., Han, P.,
902 Karion, A., Kim, J., Lopez Coto, I., Papale, D., Ramonet, M., Sperlich, P., Vardag, S. N., Vermeulen, A.,
903 Vimont, I. J., Wu, D., Zhang, W., Augusti-Panareda, A., Ahlgren, K., Ahn, D., Boyle, T., Brewer, A.,
904 Brunner, D., Cai, Q., Chambers, S., Chen, Z., Dadheech, N., D’Onofrio, C., Dunse, B. L., Engelen, R.,
905 Fathi, S., Gioli, B., Hammer, S., Hase, F., Hong, J., Hutyra, L. R., Järvi, L., Jeong, S., Karstens, U.,
906 Kenion, H. C., Kljun, N., Laurent, O., Lauvaux, T., Lin, J. C., Liu, Z., Loh, Z., Maier, F., Matthews, B.,
907 Mauder, M., Miles, N., Mitchell, L., Monteiro, V. C., Mostafavi Pak, N., Röckmann, T., Roiger, A.,
908 Roten, D., Scheutz, C., Shahrokhi, N., Shepson, P. B., Stagakis, S., Tong, X., Trudinger, C. M., Velasco,
909 E., Whetstone, J. R., Winbourne, J. B., Wu, J., Xueref-Remy, I., Yadav, V., Yu, L., Zazzeri, G., Zeng, N.,
910 and Zhou, M.: IG3IS Urban Greenhouse Gas Emission Observation and Monitoring Good Research

911 Practice Guidelines, WMO GAW Report 275, World Meteorological Organisation, Geneva, Switzerland,
912 2025.

913 U.S. Department of Agriculture, Natural Resource Conservation Service (NRCS), Indiana State Office,
914 and the Indiana Geographic Information Council (IGIC), under separate BAA Agreements in partnership
915 with the United States Geological Services (USGS) 3DEP Program. Indiana 3DEP Lidar Base Products.
916 (data set), <https://igic.memberclicks.net/indiana-s-new-3dep-lidar-data-and-informational-resources>,
917 2021.

918 Vickers, D. and Mahrt, L.: Quality Control and Flux Sampling Problems for Tower and Aircraft Data, *J*
919 *Atmos Ocean Technol*, 14, 512–526, [https://doi.org/10.1175/1520-](https://doi.org/10.1175/1520-0426(1997)014<0512:QCAFSP>2.0.CO;2)
920 [0426\(1997\)014<0512:QCAFSP>2.0.CO;2](https://doi.org/10.1175/1520-0426(1997)014<0512:QCAFSP>2.0.CO;2), 1997.

921 Vogel, E., Davis, K. J., Wu, K., Miles, N. L., Richardson, S. J., Gurney, K. R., Monteiro, V., Roest, G. S.,
922 Kenion, H. C. R., and Horne, J. P.: Using eddy-covariance to measure the effects of COVID-19
923 restrictions on CO₂ emissions in a neighborhood of Indianapolis, IN, *Carbon Manag*, 15,
924 <https://doi.org/10.1080/17583004.2024.2365900>, 2024.

925 Vogt, R., Christen, A., Rotach, M. W., Roth, M., and Satyanarayana, A. N. V.: Temporal dynamics of CO₂
926 fluxes and profiles over a Central European city, *Theor Appl Climatol*, 84, 117–126,
927 <https://doi.org/10.1007/s00704-005-0149-9>, 2006.

928 Wang, W., K. J. Davis, B. D. Cook, M. P. Butler, D. M. Ricciuto.: Decomposing CO₂ fluxes measured
929 over a mixed ecosystem at a tall tower and extending to a region: A case study, *Journal of Geophysical*
930 *Research Biogeosciences*, 111(G2), G02005, doi:10.1029/2005JG000093, 2006.

931 Ward, H. C., Rotach, M. W., Gohm, A., Graus, M., Karl, T., Haid, M., Umek, L., and Muschinski, T.:
932 Energy and mass exchange at an urban site in mountainous terrain - the Alpine city of Innsbruck, *Atmos*
933 *Chem Phys*, 22, 6559–6593, <https://doi.org/10.5194/acp-22-6559-2022>, 2022.

934 Webb, E. K., Pearman, G. I., and Leuning, R.: Correction of flux measurements for density effects due to
935 heat and water vapour transfer, *Quarterly Journal of the Royal Meteorological Society*, 106, 85–100,
936 <https://doi.org/10.1002/qj.49710644707>, 1980.

937 Wilczak, J. M., Oncley, S. P., and Stage, S. A.: Sonic Anemometer Tilt Correction Algorithms, *Boundary*
938 *Layer Meteorol*, 99, 127–150, <https://doi.org/10.1023/A:1018966204465>, 2001.

939 Wu, K., Davis, K. J., Miles, N. L., Richardson, S. J., Lauvaux, T., Sarmiento, D. P., Balashov, N. V.,
940 Keller, K., Turnbull, J., Gurney, K. R., Liang, J., and Roest, G.: Source decomposition of eddy-covariance
941 CO₂ flux measurements for evaluating a high-resolution urban CO₂ emissions inventory, *Environmental*
942 *Research Letters*, 17, <https://doi.org/10.1088/1748-9326/ac7c29>, 2022.

943 Xiao, J.F., Davis, K.J., Urban, N.M., Keller, K.: Uncertainty in model parameters and regional carbon
944 fluxes: A model-data fusion approach. *Agricultural and Forest Meteorology*, 189-190, 175-186, 2014

- 945 Xu, K., S. Metzger, A. R. Desai.: Upscaling tower-observed turbulent exchange at fine spatio-temporal
946 resolution using environmental response functions, *Agricultural and Forest Meteorology*, 232, 10-22,
947 <https://doi.org/10.1016/j.agrformet.2016.07.019>, 2017.
- 948 Yadav, V., Verhulst, K., Duren, R., Thorpe, A., Kim, J., Keeling, R., Weiss, R., Cusworth, D., Mountain,
949 M., Miller, C., and Whetstone, J.: A declining trend of methane emissions in the Los Angeles basin from
950 2015 to 2020, *Environmental Research Letters*, 18, 034004, <https://doi.org/10.1088/1748-9326/acb6a9>,
951 2023.
- 952 Yi, C., Davis, K. J., Bakwin, P. S., Berger, B. W., and Marr, L. C.: Influence of advection on
953 measurements of the net ecosystem-atmosphere exchange of CO₂ from a very tall tower, *Journal of*
954 *Geophysical Research: Atmospheres*, 105, 9991–9999, <https://doi.org/10.1029/2000JD900080>, 2000